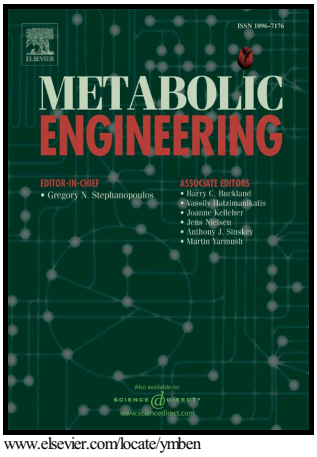

www.elsevier.com/locate/ymben

Tailored carbon partitioning for phototrophic production of (*E*)-α-bisabolene from the green microalga *Chlamydomonas reinhardtii*

Julian Wichmann, Thomas Baier, Eduard Wentnagel, Kyle J. Lauersen, Olaf Kruse

PII: S1096-7176(17)30395-6
DOI: https://doi.org/10.1016/j.ymben.2017.12.010
Reference: YMBEN1335

To appear in: *Metabolic Engineering*

Received date: 23 October 2017
Revised date: 27 November 2017
Accepted date: 11 December 2017

Cite this article as: Julian Wichmann, Thomas Baier, Eduard Wentnagel, Kyle J. Lauersen and Olaf Kruse, Tailored carbon partitioning for phototrophic production of (*E*)-α-bisabolene from the green microalga *Chlamydomonas reinhardtii*, *Metabolic Engineering,* https://doi.org/10.1016/j.ymben.2017.12.010

Tailored carbon partitioning for phototrophic production of (*E*)-α-bisabolene from the green microalga *Chlamydomonas reinhardtii*

Author names and affiliations: Julian Wichmann[1], Thomas Baier[1], Eduard Wentnagel[1], Kyle J. Lauersen[1], and Olaf Kruse[1,*]

[1]Bielefeld University, Faculty of Biology, Center for Biotechnology (CeBiTec), Universitätsstrasse 27, 33615, Bielefeld, Germany.

***Corresponding Author:** Olaf Kruse, olaf.kruse@uni-bielefeld.de

Present/Permanent address: Bielefeld University, Faculty of Biology, Center for Biotechnology (CeBiTec), Universitätsstrasse 27, 33615 Bielefeld, Germany.

Phone: +49 521 106-12258, Fax: +49 521 106-12290

Abstract

Photosynthetic microbial hosts such as cyanobacteria and eukaryotic microalgae have recently emerged as alternative engineering platforms for the sustainable light-driven bio-production of terpenoids. Many desirable compounds with numerous applications can be produced in microorganisms by heterologous expression of terpene synthases. However, success of green microbial systems has been hampered by issues such as insufficient enzyme expression titers and low flux to desired terpenoid products from carbon fixed during photosynthesis. This work demonstrates how the green microalga *Chlamydomonas reinhardtii* can be engineered to produce the sesquiterpene biodiesel precursor (*E*)-α-bisabolene. Through strategic genetic engineering, substantial enhancements of productivity were achieved by coordinated tuning of the isoprenoid metabolism, combining serial enzyme loading for terpene synthase overexpression and amiRNA-based repression of competing pathways. Up to 10.3 ± 0.7 mg bisabolene $\cdot$ g^{-1} cell dry weight could be produced in five days, which represents more than a 15-fold increase over single synthase expression strains. Investigation of strain performance in scale-up cultivations determined overall bisabolene productivity benefits from light:dark cycles. Mixotrophic cultivation can yield up to 11.0 ± 0.5 mg bisabolene per liter in seven days in these conditions, and phototrophic production of 3.9 ± 0.2 mg per liter was feasible. These achievements represent an important milestone in the engineering of *C. reinhardtii* towards the goal of designing sustainable, light-driven, green-cell algal bio-factories.

Keywords:

Microalgae. *Chlamydomonas reinhardtii*. Terpenoids. Bisabolene. amiRNA.

Abbreviations:

*Ag*Bs – *Abies grandis* bisabolene synthase

amiRNA – artificial micro ribonucleic acid

CDW – cell dry weight

IPP – isopentenyl pyrophosphate

DMAPP – dimethylallyl pyrophosphate

FPP – farnesyl pyrophosphate

GGPP – geranylgeranyl pyrophosphate

TAP – Tris Acetate Phosphate medium

TA2P – TAP medium with 2X phosphate content

T2P – TAP medium without acetate and 2X phosphate content

YFP – mVenus yellow fluorescent protein

CFP – mCerulean3 cyan fluorescent protein

RFP – mRuby2 red fluorescent protein

PQ – plastoquinone

UQ – ubiquinone

PFT – protein farnesyl transferase

AGPP – ADP-glucose pyrophosphorylase small subunit

GGPPs – geranylgeranyl pyrophosphate synthase

SQs – squalene synthase

1. Introduction

Metabolic engineering of microbial cell factories for the production of chemically diverse isoprenoid molecules has been a topic of biotechnological research for some decades and has developed into a mature technology (Ajikumar et al., 2008; Kirby and Keasling, 2009). Controlled production of isoprenoids in heterologous microbial hosts is highly valuable due to the challenging chemical synthesis or natural source limitations of these products (Misawa, 2011). Isoprenoids exhibit a wide range of potential applications in medicine (Nosten and White, 2007), food and feed (Baker and Günther, 2004; Beekwilder et al., 2014; Johnson et al., 1980), agriculture (Grace, 2002), as cosmetics (McVean and Liebler, 1999), fragrances (Ansari and Curtis, 1974), platform chemicals (Firdaus et al., 2011), and biofuels (George et al., 2015). Their modular biosynthesis begins with the C_5 building blocks isopentenyl pyrophosphate (IPP) and dimethylallyl pyrophosphate (DMAPP). Pyrophosphate synthases (prenyl transferases) catalyze the sequential condensation of IPP and DMAPP to the prenyl precursors geranyl pyrophosphate (GPP, C_{10}), farnesyl pyrophosphate (FPP, C_{15}), or geranylgeranyl pyrophosphate (GGPP, C_{20}). In nature, the highly diverse class of terpene synthases accepts these prenyl precursors and, combined with enzymes which further modify the resulting hydrocarbon skeleton, the greater variety of terpenoid structures are produced (Bohlmann et al., 1998; Keeling and Bohlmann, 2012). Isoprenoid classes are defined by the number of C_5 units: C_5 hemiterpenes, C_{10} monoterpenes, C_{15} sesquiterpenes, C_{20} diterpenes, C_{30} triterpenes, C_{40} tetraterpenes, and longer chain polyterpenes (Michal, 2012).

Isoprenoid carbon backbones are ubiquitously present in all living organisms and are involved in fulfilling a multitude of natural functions such as light harvesting, photoprotection, electron transport (as part of ubiquinone and plastoquinone), plant defense, signaling, and as membrane components (Gershenzon and Dudareva, 2007; Lange et al., 2000). This allows the transfer of terpene synthases from a source organism into a microbial host and subsequent generation of these non-native metabolites in that organism.

In contrast to fermentative microbial hosts, engineering photosynthetic unicellular green cell factories such as cyanobacteria and microalgae can allow light-driven production of isoprenoid products (Davies et al., 2015). Phototrophic cyanobacterial hosts have been used as alternative chassis for recombinant isoprenoid production already some years ago (Lindberg et al., 2010), however, only comparatively low product yields have been achieved in these systems (Davies et al., 2014; Halfmann et al., 2014). Although phototrophic systems are naturally rich in isoprenoids, carbon partitioning into these

compounds still represents only 5% of total carbon flux (Melis, 2013). Some progress has been made to overcome these limitations in cyanobacteria, which are amenable to genetic manipulation (Bentley et al., 2014; Choi et al., 2016; Formighieri and Melis, 2015; Gao et al., 2016). Eukaryotic microalgae, however, are less genetically tractable than cyanobacteria and only recently has the unicellular green alga *Chlamydomonas reinhardtii* been demonstrated to be capable of heterologous terpenoid production (Lauersen et al., 2016). The isoprenoid metabolism of *C. reinhardtii* is typical of Chlorophyta which lack the mevalonate (MVA) pathway (Lohr et al., 2012). Supply of C_5 isoprenoid precursors solely relies on the 2-C-methyl-D-erythritol 4-phosphate (MEP) pathway in the chloroplast (Fig. 1). The MVA pathway was initially contributed by the eukaryotic host during primary endosymbiosis, however, was lost throughout evolution in these organisms (Lohr et al., 2012). This metabolic structure obliges the cell to rapidly export IPP and DMAPP substrates to the cytosol by an as-of-yet unknown mechanism. These C_5 intermediates are condensed to the C_{15} FPP by the FPP synthase. FPP is the precursor for sterols, protein farnesyl tails, dolichols, and polyprenyls associated with ubiquinone (UQ) in the mitochondria.

Recently, we succeeded in engineering *C. reinhardtii* to photoautotrophically produce the FPP-derived sesquiterpene patchoulol (Lauersen et al., 2016). This was a major step forward in the engineering of eukaryotic microalgae for sustainable bio-production. However, the low titers of sesquiterpenoid achieved highlighted the need for more advanced metabolic engineering to improve product yields from this alga.

Here, we demonstrate that it is possible to conduct concerted metabolic engineering in *C. reinhardtii* and that substantial improvements in non-native isoprenoid product titers can be achieved. We show that heterologous expression of the *Abies grandis* bisabolene synthase (*Ag*Bs, (Bohlmann et al., 1998)) in *C. reinhardtii* catalyzes freely available cytosolic FPP into the sesquiterpenoid product (*E*)-α-bisabolene (hereafter: bisabolene). A repertoire of available fluorescent reporters and selection markers is used to overcome synthase titer limitations in the algal cell by serial transformation. A systematic investigation of pathways competitive for carbon in the isoprenoid pathway is presented using artificial microRNA (amiRNA)-based knock-down, revealing two carbon flux gatekeeping targets. Finally, a bisabolene production strain is described, created by combining sequential enzyme loading and amiRNA knock-down from four separate genetic constructs. Phototrophic production of bisabolene from this strain is investigated in scale-up cultivations using different carbon and light regimes.

2. Materials and Methods

2.1 *C. reinhardtii* strains and cultivations

C. reinhardtii strains UVM4 (Neupert et al., 2009) and *sta6* (Zabawinski et al., 2001), unless otherwise noted, were maintained in TAP medium (Gorman and Levine, 1965) at 150 µmol photons m^{-2} s^{-1} light intensity in shake flasks or on agar plates. Scale-up cultures were stirred in 1000 mL Erlenmeyer flasks or in 500 mL Schott bottles containing 380 mL media and 20 mL dodecane overlay. Illumination was either performed with 100 µmol photons m^{-2} s^{-1} constant light or correspondent 16:8 h light:dark cycles using either air or 3% CO_2 surface gassing. Cultivations were performed in TA2P or T2P media which differ only in the presence or absence of acetate as described (Lauersen et al., 2016). For TA2P and T2P media, pH was set to 8.

2.2 Plasmid construction, transformation, and screening of mutants

Cloning in this work was conducted using Thermo Scientific FastDigest restriction enzymes and the Rapid DNA Dephos & Ligation Kit (Roche) according to manufacturers' protocols. Q5 high fidelity polymerase with GC enhancer solution (New England Biolabs) was used to perform PCRs following manufacturer's protocols. Primers used are listed in Supplemental data file 1. All vector sequences were confirmed by sequencing (Sequencing Core Facility, CeBiTec, Bielefeld University, Germany). Plasmids were maintained in *Escherichia coli* DH5α.

The *A. grandis* bisabolene synthase (*Ag*Bs, UniProt: O81086), the *E. coli* streptomycin 3''-adenylyltransferase (*aadA*, UniProt P0AG05) and the *Streptoalloteichus hindustanus* bleomycin resistance protein (*Sh*Ble, UniProt P17493) were codon optimized by back translating the amino acid sequence and synthesized (Genscript) as previously reported (Lauersen et al., 2013). To enhance transgene expression, intron 1 of ribulose bisposphate carboxylase small subunit 2 (RBCS2) was added throughout the coding sequence as previously demonstrated (Lauersen et al., 2016). The *C. reinhardtii* codon optimized, intron containing *Ag*Bs (MG052654), *aadA* (MG052656), and *Sh*Ble (MG052655) synthetic nucleotide sequences are accessible on the NCBI database. Artificial microRNA constructs were built according to (Hu et al., 2014) with primers indicated in Supplemental data file 1.

Sequences mentioned above were designed with compatible restriction endonuclease cut sites and cloned into the pOptimized_2.0 (pOpt_2.0) vector system. This toolkit is a further developed version of the pOptimized system (Lauersen et al., 2015) with slight

modifications shown in Supplemental Figure 1. To provide a chassis for amiRNA expression, the previously described *c*CA_*g*Luc cassette (Lauersen et al., 2015) was cloned into the pOpt_2.0 backbone and modified to contain the third intron of RBCS2 (i3) as well as a *Sma*I site to allow introduction of desired amiRNA sequences (Supplemental Figure 1). All pOpt_2.0 vector backbones, including five reporter variants and template luciferase-amiRNA in four selection marker vectors have been submitted to the publicly accessible *Chlamydomonas* Resource Center as part of this work (http://chlamycollection.org/). The *Ag*Bs was cloned to create fusions with mVenus, mCerulean3, or mRuby2 fluorescent protein (Y/C/RFP) reporters. All constructs created are listed in Table 1.

Glass bead mediated transformations were performed as previously described (Kindle, 1990). Selection of positive transformants was achieved on TAP agar plates supplemented with suitable antibiotics at 10 mg L^{-1} (paromomycin), 20 mg L^{-1} (hygromycin B), 15 mg L^{-1} (zeocin), or 200 mg L^{-1} (spectinomycin) at 200 µmol photons m^{-2} s^{-1} light intensity. Colonies were maintained by stamping on TAP agar plates with respective antibiotic combinations. Expression of target constructs was identified with fluorescence microscopy for YFP, CFP, or RFP fluorescence signal on the agar plate level as previously reported (Lauersen et al., 2015). Mutants with amiRNA linked luciferase expression were selected based on bioluminescence signal captured as previously described (Lauersen et al., 2013).

Fluorescent colonies were inoculated in 24-well clear microtiter plates containing TAP medium, grown with 200 µmol photons m^{-2} s^{-1} light intensity at 180 rpm shaking to sufficient cell densities, and diluted to determine expression levels normalized to cell densities as previously described (Lauersen et al., 2016). Expression of the *Ag*Bs reporter fusions to full length was confirmed via SDS PAGE and Western blotting using either α-GFP-HRP linked antibody (Life technologies), or α-StrepII tag-HRP linked antibody (IBA Lifesciences)

2.3 Fluorescence imaging

Fluorescence microscopy was performed as previously described (Lauersen et al., 2016). Each mutant generated was additionally plated on TAP agar plates containing 250 mg L^{-1} amido black 10B to reduce background signal. After 5 d of growth with 200 µmol photons m^{-2} s^{-1} light intensity, signals for fluorescent reporters were recorded in an *in vivo* Plant Imaging System (NightShade LB985, Berthold technologies) with

respective filters for YFP (excitation: 504 nm, emission: 530 nm), CFP (excitation: 425 nm, emission: 500 nm), and RFP (excitation: 560 nm, emission: 600 nm).

2.4 Capture and analysis of bisabolene

Bisabolene productivity was screened for each genetic construct using three individual mutants each in biological triplicate. For cultivations, shake flasks with 45 mL TAP medium and 2.5 mL dodecane overlay were shaken at 120 rpm, 25 °C, and 200 µmol photons m^{-2} s^{-1} continuous light for 5 d. To harvest cultures, dodecane was removed, cell densities were measured and cell dry weight (CDW) was determined by centrifugation of 5 mL culture and drying the cell pellet at 110 ˚C overnight.

Dodecane fractions were collected by centrifugation at 20,000xg for 2 min, transferred to new sample tubes and subjected to gas chromatography-mass spectroscopy (GC-MS) analysis as previously described (Lauersen et al., 2016). Presence of bisabolene in measured samples was verified by comparison with a commercial standard (Alfa Aesar) and quantification was performed with calibration curves of serial dilutions of bisabolene in dodecane ranging from 0.5 to 450 µM (Supplemental data file 2). Due to presence of further bisabolene isomers in the commercial standard, the contribution of (*E*)-α-bisabolene to the molarity was adjusted based on an attribution of only 27.52 ± 0.27 % of total combined peak areas to the target molecule. To each sample, 250 µM α-humulene was added as internal standard. Extracted ion chromatograms of triplicate measurements were manually reviewed using mass ranges of 91.00, 93.00, and 119.00.

Product yield predictions for each strain were calculated based on reporter fluorescence per cell and the measured yield of individual strains as indicated in Supplemental data file 3.

The best performing strain expressing the *Ag*Bs-YFP fusion (construct II) was investigated for product partitioning between cell pellet, medium, and dodecane if present. Cultivations were performed under screening conditions with and without an overlay of 5% dodecane in biological triplicate. Following the regular harvesting procedure described above, the culture was centrifuged for 5 min at 3,000xg, and the obtained supernatants and cell pellets were extracted separately: supernatants were supplemented with 2.5 mL dodecane, vigorously vortexed for 1 min, and the solvent overlay was recovered and subjected to GC-MS analysis as described. Pellets were washed with bidistilled water and extracted with 1 mL dodecane by homogenization with zirconia glass beads at 6,500 rpm for 3x45 sec with 15 sec pauses in a bead-beater. Dodecane extracts were recovered and analyzed by

GC-MS as described above. Calculations for product partitioning can be found in Supplemental data file 4, productivities and their calculation for all transformants investigated are listed in Supplemental data file 5.

Strain 3X*Ag*Bs-SQs was characterized regarding growth and productivity under a range of conditions. This transformant was identified as the best performing cell line in this work and was generated by sequential transformation with constructs ii, iv, vi, and xiii (Table 1). To investigate the influence of carbon usage and light:dark cycles, scale-up cultivations were performed in Erlenmeyer flasks as single replicates as described in section 2.1. Cell densities, CDW, and bisabolene concentrations in the dodecane overlay were recorded daily. Data and calculations can be found in Supplemental data file 6.

2.5 Analysis of relative gene expression in knock-down lines

RNA was extracted from mid-log phase (24 h) grown cultures as described (Chomczynski and Sacchi, 1987). Synthesis of cDNA and subsequent quantitative real-time polymerase chain reactions (qRT-PCR) were performed with the SensiFAST™ SYBR® Hi-ROX One-Step Kit (Bioline) following manufacturer's protocols on a StepOne™ Real-Time PCR System (Applied Biosystems). Primers were designed using Primer3Plus (http://www.bioinformatics.nl/cgi-bin/primer3plus/primer3plus.cgi, (Untergasser et al., 2007)) and are indicated in Supplemental data file 1. Expression levels of targeted enzymes relative to RPL13 (ribosomal protein L13) were calculated as described previously (Livak and Schmittgen, 2001) and calculations are shown in Supplemental data file 7.

2.6 Analysis of pigment composition

To determine the content of cellular pigments, strains exhibiting a down-regulated geranylgeranyl pyrophosphate synthase (GGPPs) and a control strain expressing a secreted luciferase alone were grown to mid-log phase (48 h) in shake flasks containing 45 mL TAP medium with 100 µmol photons m^{-2} s^{-1} continuous light and 120 rpm shaking in biological triplicate. 200 µL culture was extracted with 800 µL acetone by vortexing for 10 s, followed by centrifugation for 1 min at 20,000xg, and the absorptions at wavelengths of 470 nm, 645 nm and 663 nm of the obtained supernatant were measured with a spectrophotometer. Chlorophyll a and b concentrations were calculated as described (Arnon, 1949), and total carotenoid contents were derived accordingly (Lichtenthaler and Buschmann, 2005). All values and calculations are listed in Supplemental data file 8.

2.7 Analysis of starch synthesis

To visualize starch contents at the colony level, strains were plated on TAP agar plates lacking ammonium as source of nitrogen and incubated for 2 d with 200 µmol photons m^{-2} s^{-1} continuous light. Treatment with iodine vapor allowed accumulated starch to be stained purple as previously described (Work et al., 2010).

2.8 Measurement of photosynthetic activity

Strain 3X*Ag*Bs-SQs was compared to UVM4 regarding growth pattern and photosynthetic efficiency. Both strains were grown in biological triplicate for seven days in 95 mL TAP medium with or without 5 mL dodecane overlay at 120 rpm shaking and illuminated with 200 µmol photons m^{-2} s^{-1} continuous light. Daily samples were taken for cell density and CDW measurements as described above. The chlorophyll fluorescence parameter Fv/Fm was measured using a Mini-PAM Photosynthesis Yield Analyzer (Walz Mess- und Regeltechnik). Calculations and measured values are listed in Supplemental data file 9.

2.9 Measurement of *Ag*Bs-YFP expression level during cultivation

A single *Ag*Bs-YFP expressing strain was cultivated in 500 mL Schott bottles under equal conditions as stated above (constant light only) and cell densities, CDW, bisabolene concentrations in the dodecane layer, and YFP expression per cell were recorded daily. Data and calculations are shown in Supplemental data file 10.

3. Results and Discussion

3.1 Cytosolic *Ag*Bs expression enables bisabolene production from *C. reinhardtii*.

We previously demonstrated that the cellular FPP pool of *C. reinhardtii* can be tapped to produce the non-native sesquiterpenoid patchoulol by heterologous expression of the *Pogostemon cablin* patchoulol synthase (*Pc*Ps) from the nuclear genome and localization in the cytoplasm (Lauersen et al., 2016). Here, a codon optimized *Ag*Bs was designed and 6 copies of the RBCS2i1 were spread throughout the ~2.4 kb sequence. The gene was cloned for expression in frame with YFP (Fig. 2A). After transformation, colonies could be selected by detection of the YFP signal, which was determined to be localized to the cytoplasm as intended (Fig. 2B). The full-length protein was shown to be expressed robustly (Fig. 2C, Sup. Fig. 2).

Two-phase cultivation with dodecane overlay was shown to be suitable for efficient capture of patchoulol from cell wall deficient *C. reinhardtii* (Lauersen et al., 2016). Therefore, it was also chosen here for *in situ* extraction of the more hydrophobic terpenoid product bisabolene. A cultivation with parental (WT), empty vector (YFP alone), and *Ag*Bs-YFP expressing strains was conducted, dodecane harvested and subjected to GC-MS analysis. The sesquiterpenoid product could be detected as a distinct peak, which was not observed for the WT or empty vector control strains (Fig. 2D). The peak exhibited an appropriate mass fractionation pattern relative to a bisabolene standard (Fig. 2E).

It was also important to determine the dynamics of bisabolene partitioning into the dodecane overlay, and where this product is located when the overlay is absent. A single transformant expressing the *Ag*Bs-YFP fusion was cultivated with and without a dodecane overlay (Sup. Fig. 3). The presence of the non-polar solvent significantly improved overall bisabolene yield more than five-fold compared to cultivation without dodecane (Sup. Fig. 3). The hydrophobic compound could not be found in the medium under either condition and favorably partitioned into the dodecane layer (97.6%) rather than the cell pellet (2.4%). The results demonstrate that two-phase cultivation with hydrophobic organic solvents efficiently extracts bisabolene from the algal cells and simultaneously improves productivity, which was also observed for production from yeast (Kirby et al., 2014).

3.2 Sequential transformation overcomes enzyme titer limitations.

The production of generally low titers of recombinant proteins expressed from the nuclear genome of *C. reinhardtii* is a major obstacle which has hindered proper metabolic engineering efforts with this organism (Barahimipour et al., 2015; Neupert et al., 2009).

Terpene synthase titer is often a limiting factor for efficient product generation and many studies have focused on overexpression of these enzymes by different approaches (Formighieri and Melis, 2015; Wang et al., 2016). In our previous work, low *Pc*Ps synthase titers limited productivity of patchoulol from *C. reinhardtii* and could be partially overcome by a novel strategy of gene loading (Lauersen et al., 2016). Repetitive fusions of the *Pc*Ps were used to generate synthetic proteins containing up to three active sites in one open reading frame, resulting in a four-fold increased product yield over single *Pc*Ps expression (Lauersen et al., 2016). It has also been demonstrated that fusion of a precursor producing FPP synthase to the *Pc*Ps could increase patchoulol productivity (Albertsen et al., 2011; Lauersen et al., 2016). To investigate the applicability of both strategies to the *Ag*Bs, fusion constructs with several combinations of one or two *Ag*Bs copies, the FPP synthase from *E. coli* (*ispA*), and YFP were generated and transformed into UVM4 (Sup. Fig. 4A). Although strains with full length expression of all constructs could be identified (Sup. Fig. 5), no version of the investigated fusions showed the expected increase in absolute product yields over the respective single *Ag*Bs-YFP construct (construct ii, Sup. Fig. 4B). Selected *Ag*Bs-YFP transformants yielded bisabolene up to 678.7 ± 52.7 µg g^{-1}_{CDW} (Fig. 3B). The *Ag*Bs sequence was cloned to create additional fusions with CFP in a bleomycin selection vector (Fig. 3A, iv), and with RFP in a hygromycin B selection vector (Fig. 3A, vi) to enable sequential transformation and selection cycles aimed at increasing the cellular *Ag*Bs concentration.

Introduction of a second *Ag*Bs copy fused to CFP led to a pronounced increase in production (~2.9-fold) over the parental strain, with bisabolene yields up to 1.95 ± 0.12 mg g^{-1}_{CDW} (Fig. 3B, ii+iv). Double transformation of the best single *Ag*Bs-YFP transformant with the CFP reporter only (Fig. 3A, iii) resulted in strains exhibiting slightly improved product yields of up to 1.27 ± 0.20 mg g^{-1}_{CDW} (Fig. 3B, ii+iii). Although surprising, varied expression levels of previously integrated transgenes have been observed after double transformation of *C. reinhardtii* (Lauersen et al., 2015; Rasala et al., 2014). Slight yield improvements in these empty vector control strains can be partly explained by higher levels of *Ag*Bs-YFP expression found in the mutants. The predicted yields for *Ag*Bs-YFP (yellow bars) are calculated based on reporter fluorescence per cell. However, measured yields are still higher than expected, and rearrangements in the nuclear genome caused by the induced double strand breaks during glass bead transformation might be responsible for the observed altered flux. After transforming *Ag*Bs for a third time with RFP as a reporter (Fig. 3A, vi), bisabolene yields amounted to 4.37 ± 0.73 mg g^{-1}_{CDW}

(Fig. 3B, ii+iv+vi). This represents a further ~2.2-fold improvement over the parental double mutant and the RFP control had only marginal improvements (constructs ii+iv+v). These results indicate that establishment of a strong metabolic pull is essential for high carbon flux towards the heterologous sesquiterpene product. Here, synthase titer limitations could be overcome by serial transformation of further *Ag*Bs expression constructs. Identification and characterization of novel stronger promoters as recently shown (López-Paz et al., 2017) would potentially facilitate increased terpene synthase titers in the cell and will be the subject of future investigations with these constructs.

3.3 Pathway knock-down reveals two carbon flux competitors.

Several native cellular pathways are putatively competitive for heterologous sesquiterpene production (Fig. 1). For the photosynthetic cell, the efficient capture and conversion of light energy can only be fulfilled with the aid of GGPP-derived pigments. A large fraction of IPP and DMAPP precursors is expected to be converted into the GGPP substrate, and these precursors must also leave the chloroplast for generation of FPP, the C_{15} precursor for sesquiterpenes like bisabolene. Here, the GGPP synthase (GGPPs) has been selected for knock-down (k.d.) due to its key role in terpenoid metabolism. Many other enzymes are direct competitors for the native pool of FPP, including the squalene synthase (SQs), protein farnesyl transferase (PFT), or dehydrodolichyl pyrophosphate synthase (Lohr et al., 2012). The SQs and the PFT were also selected as targets for k.d. in this work. The relative demand for farnesylated proteins for the algal cell is unclear, however, downregulation of sterol synthesis has been feasible by targeting squalene epoxidase in *C. reinhardtii* (Kajikawa et al., 2015) and has proven beneficial for sesquiterpene synthesis in other systems (Asadollahi et al., 2008; Cankar et al., 2015; Paddon et al., 2013; Peng et al., 2016; Scalcinati et al., 2012a, 2012b). The ADP-glucose pyrophosphorylase small subunit (AGPP) is the rate-limiting enzyme for generation of the main cellular storage compound starch (Zabawinski et al., 2001). AGPP may act as an additional gatekeeping enzyme limiting the available pool of glyceraldehyde 3-phosphate (G3P, Fig. 1), an immediate MEP pathway precursor. Therefore, AGPP was chosen as a fourth k.d. target for competitive analysis.

Complete knock-out of the GGPPs and the SQs (Peng et al., 2016) would be likely lethal to the algal cell. Here, we applied a previously reported technique for simultaneous rapid transformant identification and k.d. of target genes by coupling a bright, secreted luciferase to hairpin amiRNA targeting sequences (vectors viii, ix, x, and xi, Fig. 4A (Hu et al.,

2014)). Fusion of the amiRNA construct to the 3' of a luciferase permits rapid bioluminescence based screening to identify transformants with expression of the desired k.d. construct (Hu et al., 2014). The reliability of this method could be demonstrated when targeting an amiRNA against the AGPP to achieve reduction of starch synthesis (Fig. 4B). In this illustrative example, the presence of the luciferase-mediated bioluminescence signal generally coincides with an absence of starch.

Target transcript k.d. was performed in an *Ag*Bs-YFP (construct ii) + *Ag*Bs-CFP (iv) expressing strain. Three individual transformants showing robust YFP and CFP fluorescence as well as luciferase bioluminescence signal (Fig. 4C, left) were selected for each target and subjected to qRT-PCR. For all chosen strains, reduced target mRNA levels could be confirmed (Sup. Fig. 6). Resulting gravimetric yields (mg g^{-1}_{CDW}) and cellular yields (fg $cell^{-1}$) of bisabolene are shown for all mutants (Fig. 4C), and the estimated flux distribution is depicted for each target in Fig. 5. Expression of a secreted luciferase alone in an already producing strain (constructs ii+iv+vii) barely influenced yields, which on average minimally differ from expected yields calculated based on YFP and CFP reporter fluorescence (Fig. 4C, middle and right). Similar results were obtained for transformants with confirmed k.d. of the PFT (Fig. 4C, constructs ii+iv+x), likely owing to the minimal flux dedicated to this pathway in the algal cell (Fig. 5E).

Reduction in starch content by AGPP k.d. was observed to be associated with a benefit to the observed gravimetric yield of bisabolene, however, on average no clear benefit was observed at the cellular level (Fig. 4C, ii+iv+viii). This suggests that no redirection of carbon towards terpene metabolism happens at the cellular level in starch-reduced cells. Previous studies have shown generally smaller cell diameters of completely starchless mutants compared to complemented strains grown in TAP medium (Work et al., 2010). In our work, a corresponding decreased weight per cell for starch-reduced mutants was observed, resulting in increased cell densities per biomass (data not shown). Therefore, the effect is physical, rather than a modification of cellular flux towards the terpenoid product (compare Fig. 5C and B). This is in accordance with previously reported metabolic effects of complete knock-out in starch synthesis, where no redirection of the cellular metabolism was observed (Krishnan et al., 2015). The results are also similar to those of a glycogen deficient cyanobacterium which showed no benefit to bisabolene production from knock-out of the carbohydrate storage product (Davies et al., 2014).

It was questionable whether k.d. of the GGPPs would be feasible as a perturbed pigment and PQ synthesis might be lethal or physiologically adverse. However, mutants with

moderately reduced GGPPs transcript level (Sup. Fig. 6B) could be isolated and successfully cultivated in the presence of dodecane. Performance with respect to bisabolene production was clearly better than expected based on terpene synthase-linked YFP and CFP fluorescence (Fig. 4C, ii+iv+ix). Both gravimetric (88.3 ± 14.6 % benefit on average) and cellular yield improvements (92.7 ± 18.5 %) were observed. The GGPPs has a competing role for the IPP and DMAPP precursor pool, due to its k.d., these are likely diverted from the chloroplast resulting in more FPP generation in the cytoplasm (Fig. 5D).

We expected that reduction of GGPPs and consequent reduced flux towards GGPP might cause a decrease in pigment turnover. However, no correlation between a reduced GGPPs transcript abundance and the pigment content per cell could be found (Sup. Figs. 6B&7B). It is known that photosynthetic organisms exert stringent control over pigment synthesis with several key regulatory and feedback mechanisms (Cazzonelli and Pogson, 2010). In GGPP synthase k.d. strains, DXS mRNA abundance was measured and clearly reflects the amount of pigments in the cell (Sup. Fig. 7A,B). This finding suggests that DXS is a rate-limiting enzyme of terpenoid biosynthesis in *C. reinhardtii*. It is possible that there is a natural excess of GGPP available to ensure rapid adaptation of pigment turnover based on environmental conditions. Therefore, a reduction in GGPP synthase abundance might slightly reduce the GGPP pool size without affecting the flux towards carotenoids and chlorophylls, but would result in increased availability of IPP and DMAPP. The latter were shown to feedback inhibit DXS (Banerjee et al., 2013), and would consequently lower the flux through the MEP pathway. However, export from the chloroplast may relieve this inhibition and would support the diversion towards sesquiterpenes observed here (Fig. 5D).

The most significant impact on bisabolene productivity was observed by k.d. of SQs, which catalyzes the first step in the endogenous sterol pathway. Bisabolene productivity increased significantly both per gram CDW (~2.4-fold on average) and per cell (~2.1-fold) over the expected values based on *Ag*Bs-reporter expression (Fig. 4C, ii+iv+xi). This clearly demonstrated that SQs is the major competing enzyme for FPP consumption in *C. reinhardtii*. Here, k.d. of SQs increased the FPP pool size by reducing its flow to sterols (Fig. 5F), and resulted in substantially higher amounts of product. The SQs target was therefore selected for further engineering trials.

3.4 Combining increased enzyme titer and knock-down of squalene synthase for improved bisabolene productivity.

The best performing SQs k.d. strain produced 5.1 ± 0.6 mg g^{-1}_{CDW} bisabolene in screening conditions (Fig. 4C, ii+iv+xi). Similar yields were achieved with the best mutant created by triple transformation of *Ag*Bs-YFP, *Ag*Bs-CFP, and *Ag*Bs-RFP (up to 4.4 ± 0.7 mg g^{-1}_{CDW}, Fig. 3B, ii+iv+vi). Therefore, we sought to combine the maximal terpene synthase load with repression of sterol synthesis by introducing a fourth selection marker to our vector system for nuclear transgene expression. A codon optimized, RBCS2i1 intron containing *aadA* gene from *E. coli* permitted a fourth transformation in a strong triple *Ag*Bs expression strain (Fig. 6A, constructs ii+iv+vi) with the luciferase-amiRNA construct targeting the SQs (Fig. 6A, construct xiii). Three robust luciferase secreting mutants demonstrated increased production as expected in comparison to the control strain (Fig. 6B). The highest bisabolene yield achieved with these strains in screening cultivations was 10.3 ± 0.7 mg g^{-1}_{CDW}, a significant improvement over all previously generated cell lines. The quadruple mutants exhibited an average increase with respect to the predicted yield of ~1.9-fold higher than in the *Ag*Bs-YFP and -CFP containing SQs knock-down triple mutants (compare Fig. 4C, ii+iv+xi, and Fig. 6B, ii+iv+vi+xiii). This indicates that an enhanced accumulation of *Ag*Bs together with repression in sterol synthesis affects the product outcome synergistically. When SQs expression is reduced, the pool of freely available FPP precursor is obviously increased to an extent that is not completely accessible by secondary transformation with an *Ag*Bs, but can be utilized more effectively by increased enzyme titers in the quadruple mutants.

3.5 Light:dark cycles prolong exponential growth phase, increasing productivity regardless of the carbon regime.

The desire to use microalgae for bio-production processes is based on the capacity of these organisms to grow using light, CO_2, or organic carbon sources as inputs. *C. reinhardtii* can grow effectively using CO_2, acetate, or both (Sager and Granick, 1953) and different dynamics of sesquiterpene production depending on the carbon source were previously observed (Lauersen et al., 2016). A quadruple mutant (3X*Ag*Bs-SQs) which produced the highest titers of bisabolene in screening conditions (up to 4.8 ± 0.1 mg L^{-1}) was chosen for scale-up and carbon source analysis. The strain showed robust growth comparable to the parental strain with similar patterns of biomass accumulation and no altered photosystem II efficiency regardless of the presence or absence of dodecane (Sup. Fig. 8).

The 3X*Ag*Bs-SQs strain was cultivated in 380 mL volumes with a 5% dodecane overlay in either TA2P medium with air (acetate alone), T2P medium with 3% CO_2 (CO_2 alone), or

TA2P medium with 3% CO_2 (CO_2+acetate). These cultivations were performed both in constant (24 h) light and 16:8 h light:dark cycles to simulate outdoor conditions (Fig. 7).

As expected, phototrophic growth (CO_2 alone) proceeded with a linear increase of cell density, and the presence of acetate caused an exponential growth phase followed either by a stationary phase (acetate alone) or a linear phase (CO_2+acetate, Fig. 7A). For all conditions, growth was slower in light:dark regimes compared to 24 h light. Unexpectedly, bisabolene titers were higher in all light:dark cultivations compared to their 24 h counterparts regardless of the carbon source applied (Fig. 7B). Bisabolene was produced up to 11.0 ± 0.5 mg L^{-1} with CO_2+acetate (+50.3% compared to constant light), 3.9 ± 0.2 mg L^{-1} with CO_2 alone (+44.4%), and 8.0 ± 0.9 mg L^{-1} with acetate alone (+44.4%), even though higher cell densities were achieved in constant light (Fig. 7A). Bisabolene accumulation generally followed growth patterns (Fig. 7B&A), indicating that production is growth-associated. In screening conditions, acetate was used as the carbon source for mixotrophic growth in air, and smaller volumes as well as shaking were employed instead of stirring. Acetate-based production in scale-up under constant light after five days resulted in a similar productivity (4.7 ± 0.1 mg L^{-1}) compared to screening conditions (see upper paragraph), indicating the efficacy of this cultivation style.

The rate of production (Fig. 7C) peaked sharply between 48 and 72 h in constant light if acetate was present, whereas equivalent cultures maintained equally high productivities for an extended time in light:dark cycles. This indicates that a prolonged exponential growth phase and the associated presence of acetate persistently sustain the cells in a productive state, resulting in higher production titers. The highest rate achieved, however, is equal in constant light vs. light:dark cycles, which supports the view that cells reach the same maximum flux towards sesquiterpenes under either condition. In cultivations where CO_2 was present in addition to acetate, peak rates of production were also increased.

Phototrophically grown cultures exhibited lower specific production rates than mixotrophically grown ones, but productivities peaked during the same time. It was not known whether differences in expression of the terpene synthase transgene could be responsible for productivity differences observed between the carbon regimes. Therefore, normalized YFP fluorescence was measured over the cultivation time for a single *Ag*Bs-YFP expressing cell line under similar conditions in constant light. Patterns for all conditions demonstrate a peak of expression in the initial cultivation phase and were not significantly different. The only exception was observed for acetate grown cultures which

exhibited higher expression levels in the end of the culture period, however, this was not true for the CO_2 culture with additional acetate (Sup. Fig. 9).

Variations in transgene expression between these conditions cannot explain the striking differences observed in bisabolene productivities between acetate, CO_2, and CO_2+acetate grown cultures. This phenomenon must be related to different metabolic states resulting from differences in the availability of carbon and energy sources. Acetate as the major carbon source caused higher flux towards sesquiterpene product than CO_2 as the sole carbon source, but if both were abundant, productivity was highest. The potential beneficial role of acetate related respiration processes for sesquiterpene production has been discussed before (Lauersen et al., 2016). Here, further evidence is presented for this mechanism, as light:dark cycles permitted higher maximum productivities compared to constant light (2.5 ± 0.2 vs. 1.4 ± 0.1 mg g^{-1} d^{-1}) in CO_2 grown cultures. In the dark phase, cells rely on break-down of starch as energy reserve to meet their demand for ATP. This likely requires an increase in flux towards FPP to provide more UQ for respiration, potentially contributing to the observed increases in bisabolene production.

Remarkably, the best *C. reinhardtii* strain created here vastly outperforms the cyanobacterium *Synechococcus* sp. PCC 7002 which was previously engineered to produce 0.6 mg L^{-1} (0.3 mg g^{-1}_{CDW}) bisabolene in 4 d without further engineering of the terminal sesquiterpene pathway (Davies et al., 2014). The presented production capacity for bisabolene achieved in our study is clearly below the threshold for industrial feasibility and still lags behind heterotrophic hosts that are more amenable to genetic manipulation and achieve higher cell densities in shorter time. Product titers of up to 994 ± 241 mg L^{-1} with *S. cerevisiae* were reported (Peralta-Yahya et al., 2011), and the carotenogenic yeast *Rhodosporidium toruloides* was engineered to convert lignocellulosic hydrolysates to 680 mg L^{-1} bisabolene in fed-batch cultivation which could also be considered a sustainable bio-process (Yaegashi et al., 2017). It is not clear what the cellular or CDW productivities were for these organisms, as these values were not stated, so a direct comparison of the cellular metabolic capacity to our system cannot be made. Heterotrophic systems benefit from ease of high-density cultivation styles, whereas cultivation of light-driven cell systems is generally performed in more dilute cultivation set-ups. It is likely that, in addition to further improvements in cell-line engineering, advances in light-driven cultivation strategies will increase productivities of these green cell factories.

In *E. coli*, balanced expression of the heterologous mevalonate (MVA) pathway resulted in the highest reported bisabolene titer achieved to date (1.15 g L^{-1}) in shake flask cultivations

(Alonso-Gutierrez et al., 2015). In the cyanobacterium *Synechocystic* PCC 6803, expression of the MVA pathway improved the yield of heterologously produced isoprene 2.5-fold (Bentley et al., 2014). However, engineering the 7 enzymes of this pathway to express in *C. reinhardtii* will certainly be challenging. Microalgae should naturally hold significant metabolic capacity for isoprenoid products owing to their production and rapid turnover of photosynthetic related pigments. The isoprenoid rich green alga *Botryococcus braunii* var Showa channels up to 45% of its fixed CO_2 into isoprenoids and contains only the chloroplastic MEP pathway (Melis, 2013). Therefore, it is not yet clear if transfer of the MVA pathway to *C. reinhardtii* is necessary to boost productivities, or whether the native MEP pathway metabolism could be tweaked to significantly improve yields. Rate-limiting and terminal steps of sesquiterpene synthesis can still be tuned in *C. reinhardtii*. This could comprise over-expression of DXS, *B. braunii* contains three isoforms of this rate-limiting enzyme (Matsushima et al., 2012), over-expression of the IPP isomerase IDI in the chloroplast, and over-expression of the cytosolic FPP synthase.

4. Conclusions

Here, we present an advanced strategy of metabolic engineering designed to pull higher portions of precursor FPP towards a sesquiterpenoid product while simultaneously increasing the amount of precursor that is accessible. Compared to the best expressing strain created in first transformation rounds, yields could be improved more than 15-fold, demonstrating that *C. reinhardtii* has a flexible metabolism with high terpenoid turnover. It remains unclear how the FPP pool is regulated under different carbon modes in this alga and how the gap between productivities in phototrophic vs. mixotrophic growth can be closed. However, it was shown that cultivation style can greatly improve the product outcome, and additional benefits can be expected from more systematic process design optimization. Further engineering targets have to be identified to relieve the inherently stringent regulation of central carbon partitioning in this and other microalgal strains. Although here, we have overcome the bottleneck of terpene synthase titer by serial transformation, this strategy requires numerous valuable selection markers and reporters. Improvements of nuclear transgene expression, whether by strain engineering or synthetic promoters, will certainly alleviate this bottleneck. Nevertheless, this work constitutes a major milestone in the engineering of *C. reinhardtii* and serves as a starting point for future engineering towards sustainable, photosynthetic, green-cell algal bio-factories.

Acknowledgements

This project has received funding from the European Union's Horizon 2020 research and innovation program Photofuel under grant agreement No 640720 (to OK). The authors would like to express thanks to Dr. Wolfgang Hübner and Prof. Dr. Thomas Huser for conducting single-cell fluorescence microscopy, to Prof. Dr. Ralph Bock for providing strain UVM4 and to Prof. Dr. Steven Ball for providing strain *sta6*.

Conflict of Interest

The authors declare that they have no conflict of interest.

References

Ajikumar, P.K., Tyo, K., Carlsen, S., Mucha, O., Phon, T.H., Stephanopoulos, G., 2008. Terpenoids: Opportunities for Biosynthesis of Natural Product Drugs Using Engineered Microorganisms. Mol. Pharm. 5, 167–190. doi:10.1021/mp700151b

Albertsen, L., Chen, Y., Bach, L.S., Rattleff, S., Maury, J., Brix, S., Nielsen, J., Mortensen, U.H., 2011. Diversion of flux toward sesquiterpene production in *Saccharomyces cerevisiae* by fusion of host and heterologous enzymes. Appl. Environ. Microbiol. 77, 1033–40. doi:10.1128/AEM.01361-10

Alonso-Gutierrez, J., Kim, E., Batth, T.S., Cho, N., Hu, Q., Jade, L., Chan, G., Petzold, C.J., Hillson, N.J., Adams, P.D., Keasling, J.D., Garcia, H., Soon, T., 2015. Principal component analysis of proteomics (PCAP) as a tool to direct metabolic engineering. Metab. Eng. 28, 123–133. doi:10.1016/j.ymben.2014.11.011

Ansari, H.R., Curtis, A.J., 1974. Sesquiterpenes in the perfumery industry. J. Soc. Cosmet. Chem. 25, 203–231.

Arnon, D.I., 1949. Copper Enzymes in isolated chloroplasts. Polyphenoloxidase in *Beta vulgaris*. Plant Physiol. 24, 1–15.

Asadollahi, M.A., Maury, J., Møller, K., Nielsen, K.F., Schalk, M., Clark, A., Nielsen, J., 2008. Production of Plant Sesquiterpenes in *Saccharomyces cerevisiae*: Effect of *ERG9* Repression on Sesquiterpene Biosynthesis. Biotechnol. Bioeng. 99, 666–677. doi:10.1002

Baker, R., Günther, C., 2004. The role of carotenoids in consumer choice and the likely benefits from their inclusion into products for human consumption. Trends Food Sci. Technol. doi:10.1016/j.tifs.2004.04.0094

Banerjee, A., Wu, Y., Banerjee, R., Li, Y., Yan, H., Sharkey, T.D., 2013. Feedback inhibition of deoxy-D-xylulose-5-phosphate synthase regulates the methylerythritol 4-phosphate pathway. J. Biol. Chem. 288, 16926–16936. doi:10.1074/jbc.M113.464636

Barahimipour, R., Strenkert, D., Neupert, J., Schroda, M., Merchant, S.S., Bock, R., 2015. Dissecting the contributions of GC content and codon usage to gene expression in the model alga *Chlamydomonas reinhardtii*. Plant J. 84, 704–717. doi:10.1111/tpj.13033

Beekwilder, J., van Houwelingen, A., Cankar, K., van Dijk, A.D.J., de Jong, R.M., Stoopen, G., Bouwmeester, H., Achkar, J., Sonke, T., Bosch, D., 2014. Valencene synthase from the heartwood of Nootka cypress (*Callitropsis nootkatensis*) for biotechnological production of valencene. Plant Biotechnol. J. 12, 174–182. doi:10.1111/pbi.12124

Bentley, F.K., Zurbriggen, A., Melis, A., 2014. Heterologous expression of the mevalonic acid pathway in cyanobacteria enhances endogenous carbon partitioning to isoprene. Mol. Plant 7, 71–86. doi:10.1093/mp/sst134

Bohlmann, J., Crock, J., Jetter, R., Croteau, R., 1998. Terpenoid-based defenses in conifers: cDNA cloning, characterization, and functional expression of wound-inducible (*E*)-alpha-bisabolene synthase from grand fir (*Abies grandis*). Proc. Natl. Acad. Sci. U. S. A. 95, 6756–61. doi:10.1073/pnas.95.12.6756

Cankar, K., Jongedijk, E., Klompmaker, M., Majdic, T., Mumm, R., Bouwmeester, H., Bosch, D., Beekwilder, J., 2015. (+)-Valencene production in *Nicotiana benthamiana*

is increased by down-regulation of competing pathways. Biotechnol. J. 10, 180–189. doi:10.1002/biot.201400288

Cazzonelli, C.I., Pogson, B.J., 2010. Source to sink: regulation of carotenoid biosynthesis in plants. Trends Plant Sci. 15, 266–274. doi:10.1016/j.tplants.2010.02.003

Choi, S.Y., Lee, H.J., Choi, J., Kim, J., Sim, S.J., Um, Y., Kim, Y., Lee, T.S., Keasling, J.D., Woo, H.M., 2016. Photosynthetic conversion of CO2 to farnesyl diphosphate-derived phytochemicals (amorpha-4,11-diene and squalene) by engineered cyanobacteria. Biotechnol. Biofuels 9, 202. doi:10.1186/s13068-016-0617-8

Chomczynski, P., Sacchi, N., 1987. Single-Step Method of RNA Isolation by Acid Guanidinium Extraction. Anal. Biochem. 159, 156–159. doi:10.1016/0003-2697(87)90021-2

Davies, F.K., Jinkerson, R.E., Posewitz, M.C., 2015. Toward a photosynthetic microbial platform for terpenoid engineering. Photosynth. Res. 123, 265–284. doi:10.1007/s11120-014-9979-6

Davies, F.K., Work, V.H., Beliaev, A.S., Posewitz, M.C., 2014. Engineering Limonene and Bisabolene Production in Wild Type and a Glycogen-Deficient Mutant of *Synechococcus* sp. PCC 7002. Front. Bioeng. Biotechnol. 2, 21. doi:10.3389/fbioe.2014.00021

Firdaus, M., Montero De Espinosa, L., Meier, M.A.R., 2011. Terpene-based renewable monomers and polymers via thiol-ene additions. Macromolecules 44, 7253–7262. doi:10.1021/ma201544e

Formighieri, C., Melis, A., 2015. A phycocyanin · phellandrene synthase fusion enhances recombinant protein expression and β-phellandrene (monoterpene) hydrocarbons production in *Synechocystis* (cyanobacteria). Metab. Eng. 32, 116–124. doi:10.1016/j.ymben.2015.09.010

Gao, X., Gao, F., Liu, D., Zhang, H., Nie, X., Yang, C., 2016. Engineering the methylerythritol phosphate pathway in cyanobacteria for photosynthetic isoprene production from CO2. Energy Environ. Sci. 9, 1400–1411. doi:10.1039/C5EE03102H

George, K.W., Alonso-Gutierrez, J., Keasling, J.D., Lee, T.S., 2015. Isoprenoid Drugs, Biofuels, and Chemicals—Artemisinin, Farnesene, and Beyond. Adv. Biochem. Eng. / Biotechnol. 123, 127–141. doi:10.1007/10

Gershenzon, J., Dudareva, N., 2007. The function of terpene natural products in the natural world. Nat. Chem. Biol. 3, 408–414. doi:10.1038/nchembio.2007.5

Gorman, D.S., Levine, R.P., 1965. Cytochrome f and plastocyanin: their sequence in the photosynthetic electron transport chain of *Chlamydomonas reinhardi*. Proc. Natl. Acad. Sci. 54, 1665–1669. doi:10.1073/pnas.54.6.1665

Grace, M.H., 2002. Chemical composition and biological activity of the volatiles of *Anthemis melampodina* and *Pluchea dioscoridis*. Phyther. Res. 16, 183–185. doi:10.1002/ptr.872

Halfmann, C., Gu, L., Gibbons, W., Zhou, R., 2014. Genetically engineering cyanobacteria to convert CO_2, water, and light into the long-chain hydrocarbon farnesene. Appl. Microbiol. Biotechnol. 98, 9869–77. doi:10.1007/s00253-014-6118-4

Hu, J., Deng, X., Shao, N., Wang, G., Huang, K., 2014. Rapid construction and screening

of artificial microRNA systems in *Chlamydomonas reinhardtii*. Plant J. 79, 1052–1064. doi:10.1111/tpj.12606

Johnson, E.A., Villa, T.G., Lewis, M.J., 1980. *Phaffia rhodozyma* as an astaxanthin source in salmonid diets. Aquaculture 20, 123–134. doi:http://dx.doi.org/10.1016/0044-8486(80)90041-1

Kajikawa, M., Kinohira, S., Ando, A., Shimoyama, M., Kato, M., Fukuzawa, H., 2015. Accumulation of squalene in a microalga *Chlamydomonas reinhardtii* by genetic modification of squalene synthase and squalene epoxidase genes. PLoS One 10, 1–21. doi:10.1371/journal.pone.0120446

Keeling, C.I., Bohlmann, J., 2012. Wiley Encyclopedia of Chemical Biology, in: Civjan, N. (Ed.), Natural Products in Chemical Biology. John Wiley & Sons, Inc., pp. 127–142. doi:10.1002/9780470048672.wecb596

Kindle, K.L., 1990. High-frequency nuclear transformation of *Chlamydomonas reinhardtii*. Proc. Natl. Acad. Sci. USA 87, 1228–1232.

Kirby, J., Keasling, J.D., 2009. Biosynthesis of plant isoprenoids: perspectives for microbial engineering. Annu. Rev. Plant Biol. 60, 335–355. doi:10.1146/annurev.arplant.043008.091955

Kirby, J., Nishimoto, M., Chow, R.W.N., Pasumarthi, V.N., Chan, R., Chan, L.J.G., Petzold, C.J., Keasling, J.D., 2014. Use of non-ionic surfactants for improvement of terpene production in *Saccharomyces cerevisiae*. Appl. Environ. Microbiol. 80, 6685–6693. doi:10.1128/AEM.02155-14

Krishnan, A., Kumaraswamy, G.K., Vinyard, D.J., Gu, H., Ananyev, G., Posewitz, M.C., Dismukes, G.C., 2015. Metabolic and photosynthetic consequences of blocking starch biosynthesis in the green alga *Chlamydomonas reinhardtii sta6* mutant. Plant J. 81, 947–60. doi:10.1111/tpj.12783

Lange, B.M., Rujan, T., Martin, W., Croteau, R., 2000. Isoprenoid biosynthesis: the evolution of two ancient and distinct pathways across genomes. Proc. Natl. Acad. Sci. U. S. A. 97, 13172–13177. doi:10.1073/pnas.240454797

Lauersen, K.J., Baier, T., Wichmann, J., Wördenweber, R., Mussgnug, J.H., Hübner, W., Huser, T., Kruse, O., 2016. Efficient phototrophic production of a high-value sesquiterpenoid from the eukaryotic microalga *Chlamydomonas reinhardtii*. Metab. Eng. 38, 331–343. doi:10.1016/j.ymben.2016.07.013

Lauersen, K.J., Berger, H., Mussgnug, J.H., Kruse, O., 2013. Efficient recombinant protein production and secretion from nuclear transgenes in *Chlamydomonas reinhardtii*. J. Biotechnol. 167, 101–110. doi:10.1016/j.jbiotec.2012.10.010

Lauersen, K.J., Kruse, O., Mussgnug, J.H., 2015. Targeted expression of nuclear transgenes in *Chlamydomonas reinhardtii* with a versatile, modular vector toolkit. Appl. Genet. Mol. Biotechnol. 99, 3491–3503. doi:10.1007/s00253-014-6354-7

Lichtenthaler, H.K., Buschmann, C., 2005. Chlorophylls and Carotenoids: Measurement And Characterization by UV-VIS Spectroscopy. Handb. Food Anal. Chem. 2–2, 171–178. doi:10.1002/0471709085.ch21

Lindberg, P., Park, S., Melis, A., 2010. Engineering a platform for photosynthetic isoprene production in cyanobacteria, using *Synechocystis* as the model organism. Metab. Eng.

12, 70–79. doi:10.1016/j.ymben.2009.10.001

Livak, K.J., Schmittgen, T.D., 2001. Analysis of Relative Gene Expression Data Using Real-Time Quantitative PCR and the 2−ΔΔCT Method. Methods 25, 402–408. doi:10.1006/meth.2001.1262

Lohr, M., Schwender, J., Polle, J.E.W., 2012. Isoprenoid biosynthesis in eukaryotic phototrophs: a spotlight on algae. Plant Sci. 185–186, 9–22. doi:10.1016/j.plantsci.2011.07.018

López-Paz, C., Liu, D., Geng, S., Umen, J.G., 2017. Identification of *Chlamydomonas reinhardtii* endogenous genic flanking sequences for improved transgene expression. Plant J. doi:10.1111/tpj.13731

Matsushima, D., Jenke-Kodama, H., Sato, Y., Fukunaga, Y., Sumimoto, K., Kuzuyama, T., Matsunaga, S., Okada, S., 2012. The single cellular green microalga *Botryococcus braunii*, race B possesses three distinct 1-deoxy-d-xylulose 5-phosphate synthases. Plant Sci. 185–186, 309–320. doi:10.1016/j.plantsci.2012.01.002

McVean, M., Liebler, D.C., 1999. Prevention of DNA photodamage by vitamin E compounds and sunscreens: roles of ultraviolet absorbance and cellular uptake. Mol. Carcinog. 24, 169–176.

Melis, A., 2013. Carbon partitioning in photosynthesis. Curr. Opin. Chem. Biol. 17, 453–456. doi:10.1016/j.cbpa.2013.03.010

Michal, G., 2012. Biochemical Pathways: An Atlas of Biochemistry and Molecular Biology, 2nd ed. John Wiley & Sons, Inc., Hoboken, New Jersey.

Misawa, N., 2011. Pathway engineering for functional isoprenoids. Curr. Opin. Biotechnol. 22, 627–633. doi:10.1016/j.copbio.2011.01.002

Neupert, J., Karcher, D., Bock, R., 2009. Generation of *Chlamydomonas* strains that efficiently express nuclear transgenes. Plant J. 57, 1140–1150. doi:10.1111/j.1365-313X.2008.03746.x

Nosten, F., White, N.J., 2007. Artemisinin-based combination treatment of falciparum malaria. Am. J. Trop. Med. Hyg. 77, 181–192.

Paddon, C.J., Westfall, P.J., Pitera, D.J., Benjamin, K., Fisher, K., McPhee, D., Leavell, M.D., Tai, A., Main, A., Eng, D., Polichuk, D.R., Teoh, K.H., Reed, D.W., Treynor, T., Lenihan, J., Jiang, H., Fleck, M., Bajad, S., Dang, G., Dengrove, D., Diola, D., Dorin, G., Ellens, K.W., Fickes, S., Galazzo, J., Gaucher, S.P., Geistlinger, T., Henry, R., Hepp, M., Horning, T., Iqbal, T., Kizer, L., Lieu, B., Melis, D., Moss, N., Regentin, R., Secrest, S., Tsuruta, H., Vazquez, R., Westblade, L.F., Xu, L., Yu, M., Zhang, Y., Zhao, L., Lievense, J., Covello, P.S., Keasling, J.D., Reiling, K.K., Renninger, N.S., Newman, J.D., 2013. High-level semi-synthetic production of the potent antimalarial artemisinin. Nature 496, 528–532. doi:10.1038/nature12051

Peng, B., Plan, M.R., Chrysanthopoulos, P., Hodson, M.P., Nielsen, L.K., Vickers, C.E., 2016. A squalene synthase protein degradation method for improved sesquiterpene production in *Saccharomyces cerevisiae*. Metab. Eng. 39, 209–219. doi:10.1016/j.ymben.2016.12.003

Peralta-Yahya, P.P., Ouellet, M., Chan, R., Mukhopadhyay, A., Keasling, J.D., Lee, T.S., 2011. Identification and microbial production of a terpene-based advanced biofuel.

Nat. Commun. 2, 1–8. doi:10.1038/ncomms1494

Rasala, B.A., Chao, S.S., Pier, M., Barrera, D.J., Mayfield, S.P., 2014. Enhanced genetic tools for engineering multigene traits into green algae. PLoS One 9, 1–8. doi:10.1371/journal.pone.0094028

Sager, B.R., Granick, S., 1953. Nutritional studies with *Chlamydomonas reinhardtii*. Ann. N. Y. Acad. Sci. 56, 831–838. doi:10.1111/j.1749-6632.1953.tb30261.x

Scalcinati, G., Knuf, C., Partow, S., Chen, Y., Maury, J., Schalk, M., Daviet, L., Nielsen, J., Siewers, V., 2012a. Dynamic control of gene expression in *Saccharomyces cerevisiae* engineered for the production of plant sesquitepene α-santalene in a fed-batch mode. Metab. Eng. 14, 91–103. doi:10.1016/j.ymben.2012.01.007

Scalcinati, G., Partow, S., Siewers, V., Schalk, M., Daviet, L., Nielsen, J., 2012b. Combined metabolic engineering of precursor and co-factor supply to increase alpha-santalene production by Saccharomyces cerevisiae. Microb. Cell Fact. 11, 1–16. doi:10.1186/1475-2859-11-117

Untergasser, A., Nijveen, H., Rao, X., Bisseling, T., Geurts, R., Leunissen, J.A.M., 2007. Primer3Plus, an enhanced web interface to Primer3. Nucleic Acids Res. 35, 71–74. doi:10.1093/nar/gkm306

Wang, X., Liu, W., Xin, C., Zheng, Y., Cheng, Y., Sun, S., Li, R., Zhu, X.-G., Dai, S.Y., Rentzepis, P.M., Yuan, J.S., 2016. Enhanced limonene production in cyanobacteria reveals photosynthesis limitations. Proc. Natl. Acad. Sci. 113, 14225–14230. doi:10.1073/pnas.1613340113

Work, V.H., Radakovits, R., Jinkerson, R.E., Meuser, J.E., Elliott, L.G., Vinyard, D.J., Laurens, L.M.L., Dismukes, G.C., Posewitz, M.C., 2010. Increased lipid accumulation in the *Chlamydomonas reinhardtii sta7-10* starchless isoamylase mutant and increased carbohydrate synthesis in complemented strains. Eukaryot. Cell 9, 1251–1261. doi:10.1128/EC.00075-10

Yaegashi, J., Kirby, J., Ito, M., Sun, J., Dutta, T., Mirsiaghi, M., Sundstrom, E.R., Rodriguez, A., Baidoo, E., Tanjore, D., Pray, T., Sale, K., Singh, S., Keasling, J.D., Simmons, B.A., Singer, S.W., Magnuson, J.K., Arkin, A.P., Skerker, J.M., Gladden, J.M., 2017. *Rhodosporidium toruloides*: a new platform organism for conversion of lignocellulose into terpene biofuels and bioproducts. Biotechnol. Biofuels 10, 1–13. doi:10.1186/s13068-017-0927-5

Zabawinski, C., Koornhuyse, N. van den, D'Hulst, C., Schlichting, R., Giersch, C., Delrue, B., Lacroix, J.-M., Preiss, J., Ball, S., 2001. Starchless Mutants of *Chlamydomonas reinhardtii* Lack the Small Subunit of a Heterotetrameric ADP-Glucose Pyrophosphorylase. J. Bacteriol. 183, 1069–1077. doi:10.1128/JB.183.3.1069

Figures

Figure 1 Isoprenoid metabolism in *C. reinhardtii*. The chloroplast harbors the 2-*C*-methyl-D-erythritol 4-phosphate (**MEP**) pathway which supplies the C_5 building blocks isopentenyl pyrophosphate (**IPP**) and dimethylallyl pyrophosphate (**DMAPP**). Unknown transporters (**T?**) may be responsible for export from the chloroplast to the cytosol where farnesyl pyrophosphate (**FPP**) is generated by its synthase (**FPPs**). A non-native sesquiterpenoid product is synthesized here from FPP by overexpression of the *Abies grandis* bisabolene synthase (***Ag*Bs**) (chemical structure depicted). Abbreviations: **CBB** Calvin-Benson-Bassham cycle, **AGPP** ADP-glucose pyrophosphorylase small subunit (UniProt ID: Q9LLL6), **DXS** 1-deoxy-D-xylulose 5-phosphate synthase (O81954), **IDI** isopentenyl pyrophosphate:dimethylallyl pyrophosphate isomerase (A8JF38). **GGPPs** geranylgeranyl pyrophosphate synthase (A8JHU6), product: geranylgeranyl pyrophosphate (C_{20}). **PSY** phytoene synthase (Q6J214), product: phytoene (C_{40}). **GGR** geranylgeranyl reductase (A8HNE8). **SPPs** solanesyl pyrophosphate synthase (A8HRQ4), product: solanesyl pyrophosphate (C_{45}). **FPPs** farnesyl diphosphate synthase (A8IX41), product: farnesyl pyrophosphate (C_{15}). **PPPs** polyprenyl diphosphate synthase (A8HX47, Phytozome v5.5, termed FPP specific PPs). **SQs** squalene synthase (A8IE29). **PFT** protein farnesyl transferase (A8JAL7). **DeDolPs** dehydrodolichyl pyrophosphate synthases I & II (A8JCC5 & A8HX47). **G3P** glyceraldehyde 3-phosphate. Dotted lines - transport, dashed lines - a series of reactions, bold lines - single enzymatic reactions. Enzyme abbreviations in blue.

Figure 2 Fusion of the mVenus (YFP) to a synthetic codon-optimized, intron containing *Ag*Bs (**A**) and its efficient expression in the algal cytoplasm. **B** Fluorescence microscopy images of parental strain (WT), and representative individual cells expressing YFP or the *Ag*Bs-YFP fusion. Individual filter signals are indicated (**chloro** chlorophyll signal **DIC** differential interference contrast). Scale bars represent 5 µm. **C** Western blot of total cellular protein with an α-GFP antibody. Ponceau S loading control shown. *Ag*Bs-YFP expressing strains (1-4) exhibit signals at the appropriate predicted molecular mass (~124.0 kDa). M - marker. Detected proteins run ~20 kDa lower than predicted due to previously observed protein breakage of the YFP expressed in *C. reinhardtii* (Lauersen et al., 2016). **D** Extracted-ion GC-MS chromatograms of bisabolene standard (Std.) dissolved in dodecane (450 µM) and dodecane overlays harvested from 5 d shake flask cultivations of the strains indicated in B (m/z 91.00, 93.00, and 119.00). All dodecane samples contain

250 µM α-humulene as internal standard, visible as a peak at 13.7 min retention time. **E** The peak at 15.6 min retention time obtained for *Ag*Bs expressing mutants exhibits mass fractionation identical to that of bisabolene standard (lower panel).

Figure 3 Enhanced *Ag*Bs protein accumulation increases product yield. **A** Expression vectors for fluorescent reporters CFP and RFP (iii and v), and *Ag*Bs fused to YFP (ii), CFP (iv), or RFP (vi). Selection markers are indicated as Paro (paromomycin), Ble (bleomycin), and Hyg (hygromycin B). **B** Performance of strains generated through sequential transformations. Three robust expressing mutants identified in each transformation round were analyzed for bisabolene yield. Vector (ii) was first transformed into UVM4 (WT), resulting in *Ag*Bs-YFP expressing colonies. This was followed by transformation of the best producing mutant with either construct (iii) or (iv). The best double transformant (constructs ii+iv) was again transformed with either vector (v) or vector (vi), resulting in triple transformants. Signals obtained from the pictured (P) colonies with YFP (Y), CFP (C), and RFP (R) filters are shown. Measured bisabolene yields are represented by grey bars. Based on measured expression level of each reporter, yield predictions are made assuming a linear correlation between productivity and enzyme titer (Lauersen et al., 2016). The predicted cumulative yield partition for YFP (yellow bars), CFP (blue), and RFP (red) is depicted with transparent color bar overlays. Error bars represent 95% confidence intervals. **C** Representative extracted-ion GC-MS chromatograms depict increased peak areas of the product with each further introduced *Ag*Bs.

Figure 4 Identification of gatekeeping enzymes for sesquiterpene production by rapid competitive pathway knock-down. **A** Vectors used for expression of *Ag*Bs fused to YFP (ii) or CFP (iv) and amiRNA-mediated k.d. of putatively competitive enzymes: the ADP-glucose pyrophosphorylase small subunit (AGPP, construct viii), the geranylgeranyl pyrophosphate synthase (GGPPs, ix), the protein farnesyl transferase (PFT, x), and the squalene synthase (SQs, xi). Reduction in mRNA abundance of these targets was confirmed by qRT-PCR (Sup. Fig. 6). K.d. strains can be more rapidly identified using the simultaneously secreted luciferase as shown in **B**: luciferase bioluminescence signal (left picture) of mutants expressing construct viii (AGPP#3, 12, 11, 5) reliably correlates to reduction in starch content as visualized by an iodine vapor staining (right picture). Starch is dyed purple with this method and mutants reduced in starch remain green typified in the

completely starchless mutant *sta6* (Zabawinski et al., 2001). Starch is still present in the parental strain, a strain expressing the luciferase alone (construct vii), and mutants with no detectable bioluminescence signal (AGPP#13). **C** (left side) reporter phenotypes in colonies on agar plates: color photograph (P), YFP and CFP fluorescence signals (Y, C), luciferase bioluminescence signal (L), as well as iodine staining are shown for each strain. **C** (middle and right sections) bisabolene yields are depicted in bar graphs. For each combination of genetic constructs (indicated on the far left), three individual mutants were chosen for two-phase cultivation in biological triplicate. Product titers determined by GC-MS of the harvested dodecane overlays were used to calculate gravimetric yields (mg g_{CDW}^{-1}) and cellular yields (fg $cell^{-1}$) shown in purple. Yield predictions based on YFP and CFP signals were calculated as in Fig. 3 (yellow and blue bars, respectively), allowing calculation of average deviations from the measured yields (thick purple bars). Error bars represent 95% confidence intervals.

Figure 5 Carbon flux distribution for individual investigated knock-downs. Arrow thickness suggests an approximate flux. **A** The WT cell. **B** The *Ag*Bs diverts FPP to produce bisabolene. **C** Starch synthesis k.d. results in smaller cells, but no repartitioning of central carbon towards terpenoids. **D** GGPPs k.d. increases IPP and DMAPP export from the chloroplast, yielding more bisabolene. **E** PFT k.d. has no influence on flux distribution. **F** SQs k.d. increases the FPP pool size, redirecting carbon towards bisabolene. Abbreviations according to Fig. 1: $\mathbf{C_3}$ G3P and pyruvate, $\mathbf{C_5}$ IPP and DMAPP, $\mathbf{C_{15}}$ FPP, $\mathbf{C_{20}}$ GGPP.

Figure 6 Combination of *Ag*Bs loading with SQs k.d. and its effect on yield. **A** Constructs ii, iv, and vi were sequentially transformed into strain UVM4 to maximize expression of the *Ag*Bs first. Quadruple transformants were then created with either a secreted luciferase alone (construct xii) or the SQs amiRNA (construct xiii). Selection markers: Paro (paromomycin), Ble (bleomycin), Hyg (hygromycin B), and Spect (spectinomycin). **B** Mutant phenotypes and gravimetric product yields for all parental strains and three individual mutants of each luciferase based construct are presented as in Fig. 4C. Error bars represent 95% confidence intervals.

Figure 7 Scale-up, growth behavior, and productivities of a quadruple transformed *C. reinhardtii* with 3X*Ag*Bs-FP expression constructs and k.d. of SQs. 400 mL batch

cultivations were performed with different carbon sources and either 100 µmol photons m^{-2} s^{-1} constant light (upper panel) or correspondent 16:8 h light:dark cycles (lower panel, dark phases indicated). Modified media were used with a 5% dodecane overlay to capture bisabolene. Acetate, 3% CO_2, or acetate and CO_2 served as carbon sources. Cell densities (**A**) and bisabolene product titers from the dodecane overlay measured by GC-MS (**B**) are shown. Normalization to cell dry weight (data not shown) permitted calculation of specific production rates (**C**) from each carbon source.

Supplemental Figures

Supplemental Figure 1 Vector systems used in this work with restriction endonuclease sites and genetic elements indicated. Compared to the pOptimized vectors (**A**, (Lauersen et al., 2015)), the pOptimized_2.0 vectors (**B**) were developed to contain further cut sites and a reduced multiple cloning site (indicated in bold letters). The repertoire of antibiotic resistance cassettes was extended by two additional genes, the *Sh*Ble encoding the *Streptoalloteichus hindustanus* bleomycin resistance protein (UniProt P17493) and the *aadA* encoding the *E. coli* streptomycin 3''-adenylyltransferase (UniProt P0AG05), each assigned with the RBCS2 intron 1 (i1). **C** The *c*CA_*g*Luc cassette described earlier (Lauersen et al., 2015) was cloned into the pOptimized_2.0 backbone. The RBCS2 intron 3 (i3) was amplified with primers i3FwEcoRVTAA and i3RvSmaIEcoRI (Supplemental data file 1) to contain a 5' stop codon and an additional *Sma*I cut site, and cloned into vectors pOpt2_*c*CA_*g*Luc for each respective antibiotic. Sequences encoding artificial microRNAs assembled via PCR were cloned into the obtained vector using *Sma*I-*Eco*RI. Each amiRNA consists of a sense and antisense region connected by a hairpin structure constructed as previously described (Hu et al., 2014).

Supplemental Figure 2 Sequentially transformed mutants expressing *Ag*Bs-reporter fusions (Fig. 3 A, constructs II, IV, and VI) demonstrate protein products at the appropriate predicted molecular mass (~124.0 kDa). Total cellular proteins were run on 10% SDS PAGE gels and subjected to Western blotting with an α-StrepII tag antibody. All constructs receive the StrepII tag from the pOptimized_2.0 vector backbone as with the original vectors (Lauersen et al., 2015). UVM4 parental strain (**P**) and strain expressing the mVenus (YFP) reporter alone (**C**) are shown as controls. Ponceau S stain is shown on the nitrocellulose membrane as a loading control. **M** - PageRuler™ Prestained Protein Ladder (Thermofisher Scientific). **1** *Ag*Bs-YFP (construct II, Fig. 3A) expressing strain. **2-4** *Ag*Bs-YFP and *Ag*Bs-CFP (constructs II and IV, Fig. 3A) expressing double mutants. **5-7** *Ag*Bs-YFP, *Ag*Bs-CFP, and *Ag*Bs-RFP (constructs II, IV, and VI, Fig. 3A) expressing triple transformants. Due to overlapping molecular masses of the *Ag*Bs-YFP, *Ag*Bs-CFP, and *Ag*Bs-RFP protein products, fluorescence images are shown for respective double and triple transformants in Fig. 3 to confirm simultaneous presence of each indicated reporter.

Supplemental Figure 3 Product partitioning between cell pellet, culture medium (supernatant), and dodecane overlay in the presence or absence of overlay during

cultivation of an *Ag*Bs-YFP expressing transformant (construct II, Fig. 3A). Cultivation was performed for 5 d in TAP medium and cultures were harvested as described in the Material and Methods section. Error bars represent 95% confidence intervals of biological triplicates.

Supplemental Figure 4 Attempts to perform gene loading with the *Ag*Bs, including fusion to the *ispA* FPP synthase from *E. coli*. Three individual mutants for each construct (**A**) were cultivated with a 5% dodecane overlay for 5 d in TAP medium in biological triplicate. Yields of bisabolene obtained per gram cell dry weight (**B**) were normalized to the cellular YFP expression level (YFP fluorescence per cell) to show effects of enzyme fusions on relative enzyme activity (**C**). Error bars represent 95% confidence intervals of three individual strains, each cultivated in biological triplicate. Each mutant was confirmed to express the indicated fusion construct to full length by Western blotting (Sup. Fig. 5).

Supplemental Figure 5 Full-length protein product detection in selected strains transformed with the vectors depicted in Sup. Fig. 4. 10% SDS PAGE gels with total cellular proteins were run and subjected to Western blotting with α-GFP antibody. As loading control, Ponceau S stain is shown on the nitrocellulose membrane. **Upper panel**: M – marker, WT – parental strain UVM4. Three out of 8 investigated mutants (#1, 3, and 8) exhibit a protein product of correct size (~218.1 kDa) for a 2X*Ag*Bs-YFP fusion (construct xiv). Others expressed only partial products. **Middle panel**: individual strains expressing the *ispA*-*Ag*Bs-YFP (1-4, construct xv) or the *Ag*Bs-*ispA*-YFP fusions (5-8, construct xvi). All exhibit a band at the predicted apparent molecular mass of ~156 kDa. Mutants 1,2,3 and 5,7,8 were chosen for further analysis (shown in Sup. Fig. 4). 1X – *Ag*Bs-YFP (construct ii), 2X – 2X*Ag*Bs-YFP (construct xiv, colony 3, upper panel). **Lower panel**: transformants expressing fusions with an expected molecular mass of ~249.9 kDa. 1-4 – *ispA*-2X*Ag*Bs-YFP (construct xvii), 5-8 – 2X*Ag*Bs-*ispA*-YFP (construct xviii), 9-12 – *Ag*Bs-*ispA*-*Ag*Bs-YFP (construct xix). For construct xviii, mutant 6, expression was below the limit of detection by Western blotting, however, bisabolene productivity appropriate for full-length expression was measured (Sup. Fig. 4 C). All proteins detected here run ~20 kDa lower than predicted due to protein breakage in the YFP which has been previously observed for recombinant proteins expressed in *C. reinhardtii* (Lauersen et al., 2016).

Supplemental Figure 6 Messenger RNA levels of genes targeted for amiRNA-mediated knock-down. Expression intensity of 3 individual mutants relative to the control strain is shown for each amiRNA construct. In addition to the *Ag*Bs-reporter fusions (constructs ii+iv), the control strain expresses a secreted luciferase alone (construct vii), whereas all transformants exhibiting a knock-down express a luciferase-amiRNA fusion (constructs viii, ix, x, and xi, respectively) directed against the different mRNA targets: the ADP-glucose pyrophosphorylase small subunit (**A**), the geranylgeranyl pyrophosphate synthase (**B**), the protein farnesyl transferase (**C**), and the squalene synthase (**D**). Error bars represent 95% confidence intervals of biological duplicates measured in technical triplicates.

Supplemental Figure 7 Comparison of 1-deoxy-D-xylulose 5-phosphate synthase (DXS) expression level and cellular pigment content of cell lines demonstrating a GGPPs knock-down (constructs ii+iv+ix) relative to the respective control strain expressing only secreted luciferase without a hairpin amiRNA target (constructs ii+iv+vii). Error bars represent 95% confidence intervals (biological triplicates).

Supplemental Figure 8 Growth pattern comparison of UVM4 and the 3X*Ag*Bs-SQs expression strain with and without an overlay of dodecane in shake flasks. Daily recorded cell densities (**A)**, CDW (**B**), and values for Fv/Fm (**C)** are shown for the time course of the cultivation. Error bars represent 95% confidence intervals of biological triplicates.

Supplemental Figure 9 Comparison of *Ag*Bs-YFP expression level measured as YFP fluorescence per cell during cultivations with different carbon regimes in 24 h light. A single *Ag*Bs-YFP expressing strain was grown in 380 mL modified medium (Lauersen et al., 2016) and a 5% overlay of dodecane with either acetate alone as the sole carbon source (surface gassing with air), 3% CO_2 as the sole carbon source, or both 3% CO_2 and acetate. Error bars represent 95% confidence intervals of biological triplicates.

Supplemental data file captions

Supplemental data files 1-10 – Wichmann et al 2017 – Tailored carbon partitioning for phototrophic production of (*E*)-α-bisabolene from the green microalga *Chlamydomonas reinhardtii*.zip Contains Supplemental data files 1-10

Supplemental data file 1 - Primers used in this study A list of primers used for cloning of genetic constructs and for qRT-PCR as listed in Table 1.

Supplemental data file 2 - Bisabolene standard calibration Calculations for bisabolene standard quantification.

Supplemental data file 3 - Yield predictions Equations used for calculation of predicted bisabolene yields based on cellular fluorescent reporter signals as shown in Fig. 3, 4, and 6.

Supplemental data file 4 - Product partitioning Calculations for bisabolene partitioning between cell pellet, culture medium, and dodecane overlay as shown in Sup. Fig. 3.

Supplemental data file 5 - Productivities of all transformants Calculation of bisabolene titers and yields for all mutants created in this work as shown in Sup. Fig. 4 and Fig. 3, 4, and 6.

Supplemental data file 6 - Growth curves and productivities of scale-up cultivations Cell densities, CDW, and calculation of bisabolene titers and production rates for scale-up cultivations of 3X*Ag*Bs-SQs mutant as shown in Fig. 7.

Supplemental data file 7 - Relative mRNA levels of knock-down mutants Calculation of relative expression levels of genes targeted for knock-down as shown in Sup. Fig. 6.

Supplemental data file 8 - DXS expression and pigments in GGPPs knock-downs Calculation of relevant data visualized in Sup. Fig. 7.

Supplemental data file 9 - Growth curves of UVM4 and 3XAgBs-SQs strain Cell densities, CDW, and Fv/Fm values for cultivations with and without dodecane of WT and strain 3X*Ag*Bs-SQs as shown in Sup. Fig. 8.

Supplemental data file 10 - *Ag*Bs-YFP expression level during cultivation Cell densities, CDW, and calculation of cellular YFP fluorescence intensities in different carbon regimes for *Ag*Bs-YFP expressing strain as visualized in Sup. Fig. 9.

Tables

Table 1: Genetic constructs used in this study

Construct name	Vector	Antibiotic resistance in *C. reinhardtii*	Gene length with introns from start codon to stop (bp)	CDS (bp)	RBCS2 i1 copies	Protein length (aa)	Predicted molecular weight (kDA)	Accession No. (NCBI)
pOpt2_mVenus_Paro	**i**	paromomycin	1287	813	1	270	30.6	KM061060*
*Ag*Bs-YFP	**ii**	paromomycin	4605	3261	7	1086	124.2	cloned in v:**i**
pOpt2_mCerulean3_Ble	**iii**	zeocin	1287	813	1	270	30.4	KM061066*
*Ag*Bs-CFP	**iv**	zeocin	4605	3261	7	1086	124.0	v:**iii**
pOpt2_mRuby2_Hyg	**v**	hygromycin B	1281	807	1	268	30.2	KM061068*
*Ag*Bs-RFP	**vi**	hygromycin B	4605	3261	7	1086	124.0	v:**v**
pOpt2_*c*CA_*g*Luc_i3_Hyg	**vii**	hygromycin B	1104	630	1	209	22.5	KM061064*
amiAGPP_3'	**viii**	hygromycin B	1104	630	1	209	22.5	v:**vii**
amiGGPPs_3'	**ix**	hygromycin B	1104	630	1	209	22.5	v:**vii**
amiPFT_3'	**x**	hygromycin B	1104	630	1	209	22.5	v:**vii**
amiSQs_3'	**xi**	hygromycin B	1104	630	1	209	22.5	v:**vii**
pOpt2_*g*Luc_i3_Spect	**xii**	spectinomycin	1104	630	1	209	22.5	KM061064*
amiSQs_3'_Spect	**xiii**	spectinomycin	1104	630	1	209	22.5	v:**xii**
2X*Ag*Bs-YFP	**xiv**	paromomycin	7929	5715	13	1904	218.1	v:**i**
ispA-*Ag*Bs-YFP	**xv**	paromomycin	5783	4149	9	1382	156	v:**i**
*Ag*Bs-*ispA*-YFP	**xvi**	paromomycin	5783	4149	9	1382	156	v:**i**
ispA-2X*Ag*Bs-YFP	**xvii**	paromomycin	9107	6603	15	2200	249.9	v:**i**
2X*Ag*Bs -*ispA*-YFP	**xviii**	paromomycin	9107	6603	15	2200	249.9	v:**i**
*Ag*Bs-*ispA*-*Ag*Bs-YFP	**xix**	paromomycin	9107	6603	15	2200	249.9	v:**i**
		UniProt ID						
*Ag*Bs alone		O81086	3318	2448	6	816	93.6	MG052654
ispA alone		P22939	1184	894	2	298	32.0	KX097888
*Sh*Ble alone		P17493	526	381	1	126	14.0	MG052655
aadA (Spect) alone		P0AG05	937	792	1	263	29.3	MG052656

***Vector sequence available through NCBI, modified as described in the text**

Note: 1 copy of the RBCS2 intron 1 (i1) is found within the HSP70-RBCS2 promoter. In addition, all YFP-, CFP-, or RFP linked constructs contain the RBCS2i2 intron in the fluorescent reporter as in Lauersen et al., 2015 Targeted expression of nuclear transgenes in *Chlamydomonas reinhardtii* with a versatile, modular vector toolkit. AMAB. 99(8) 3491-3503.

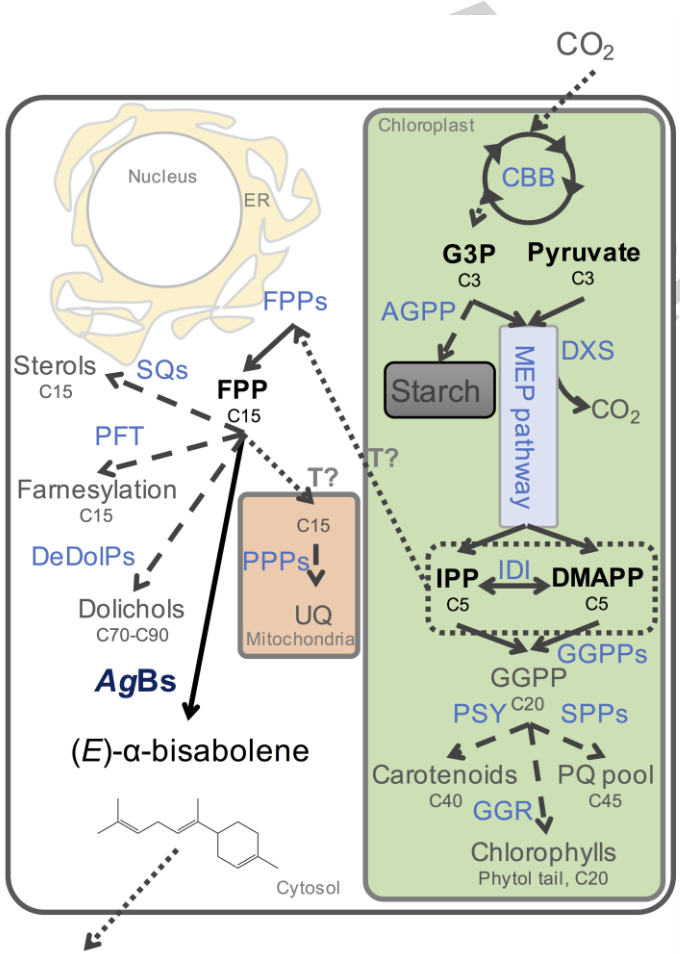

Fig. 1

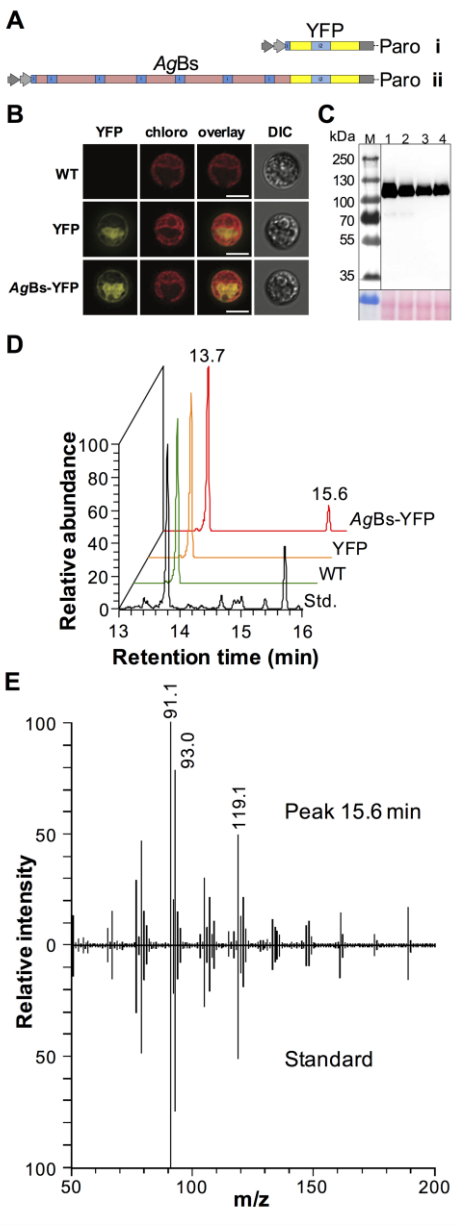

Fig. 2

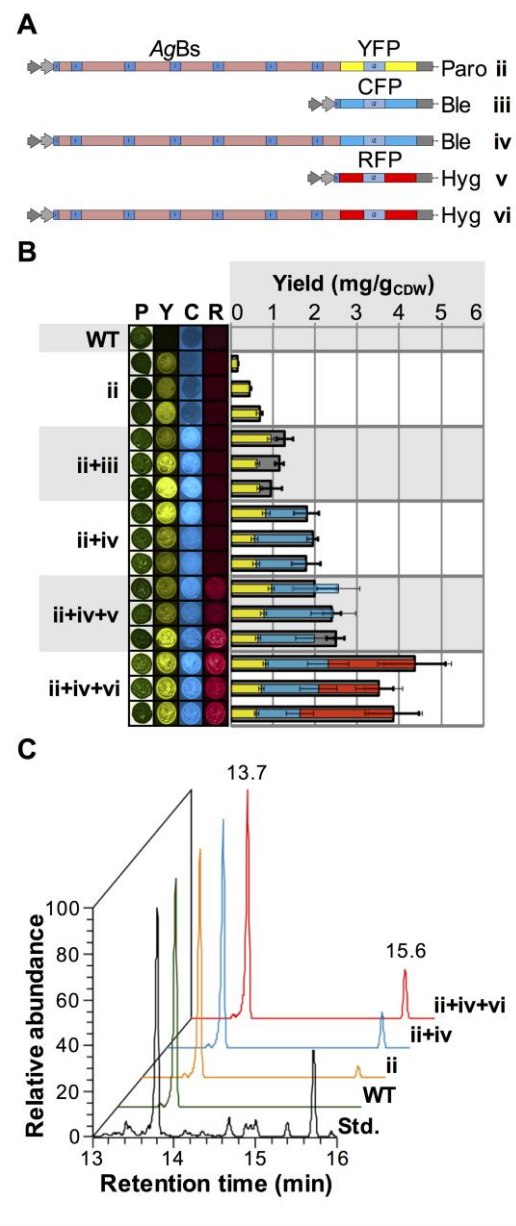

Fig. 3

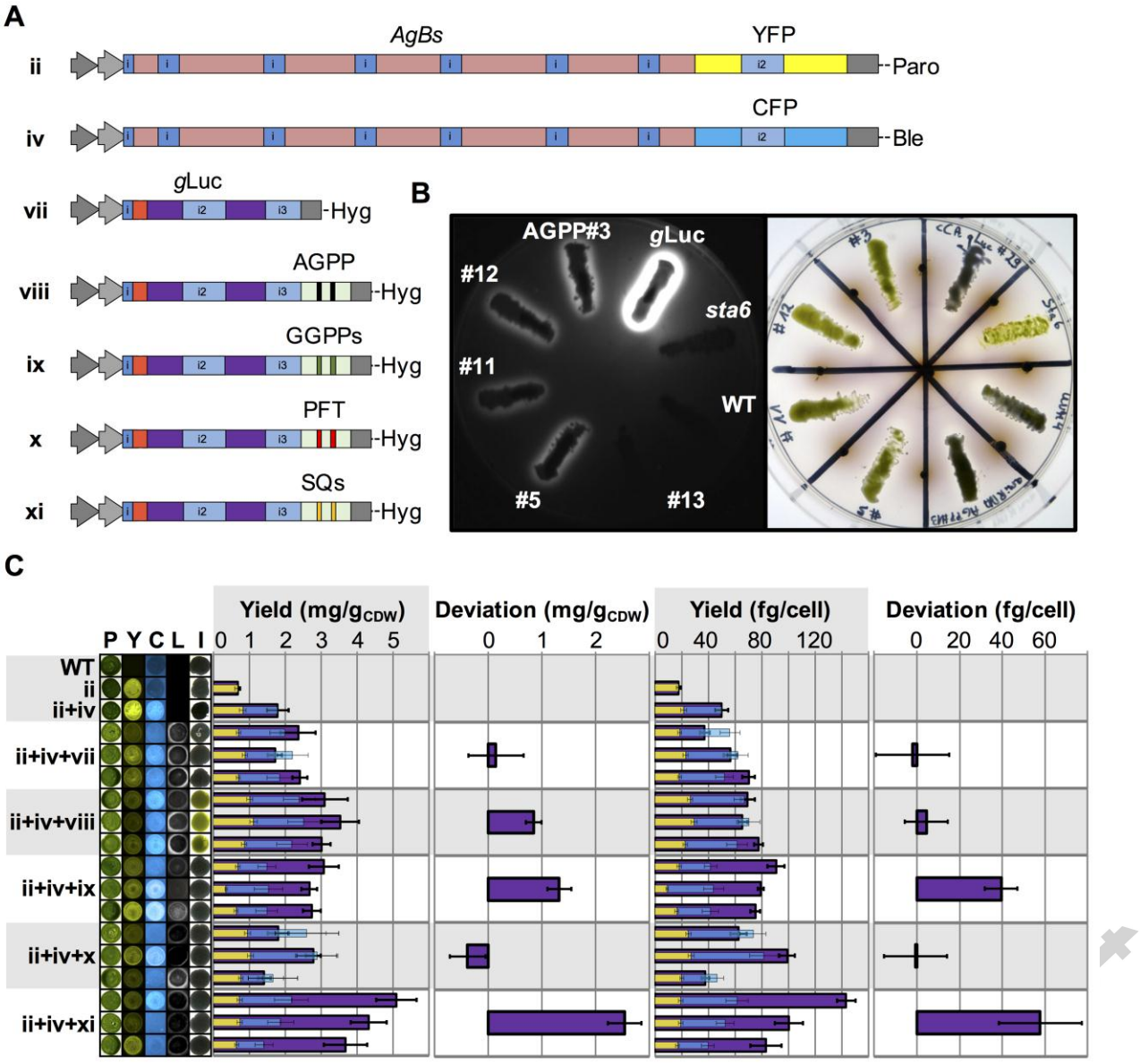

Fig. 4

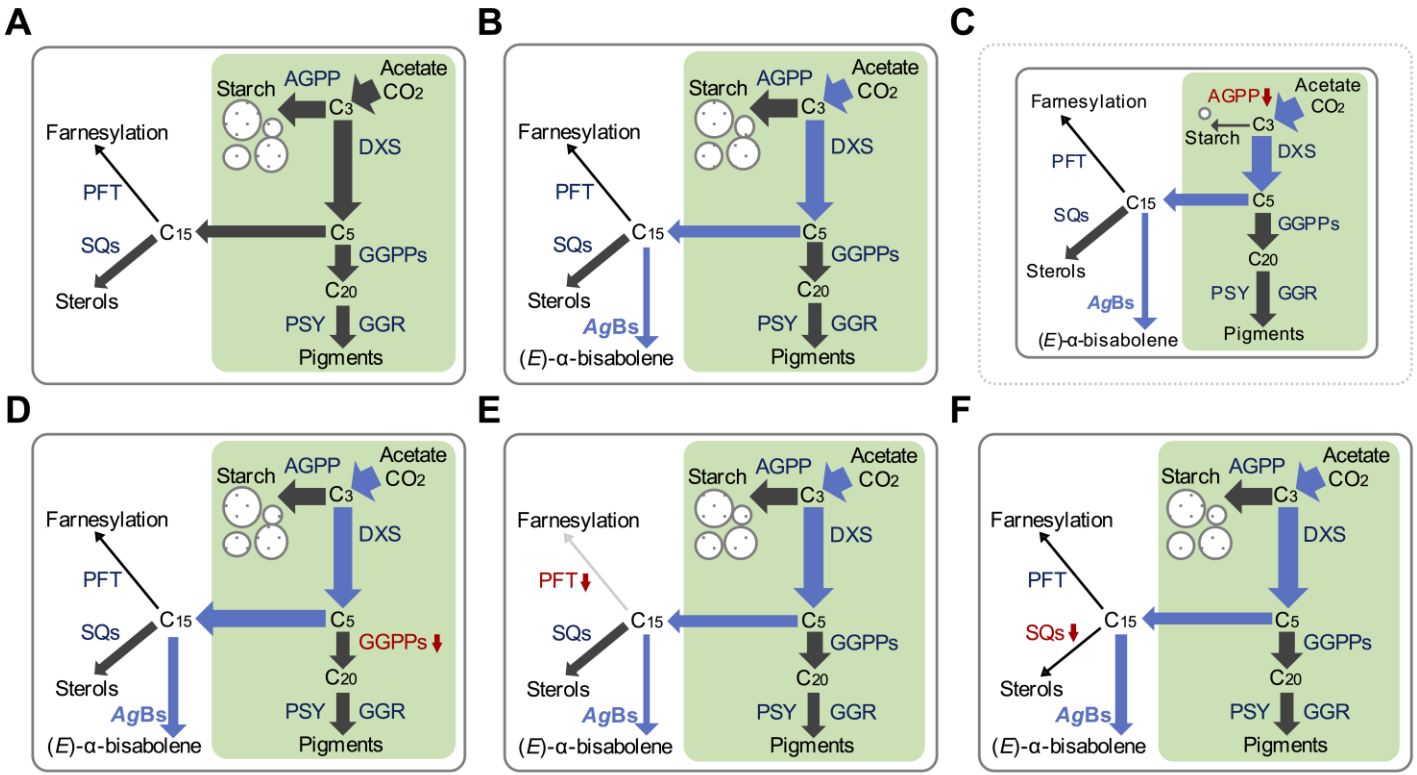

Fig. 5

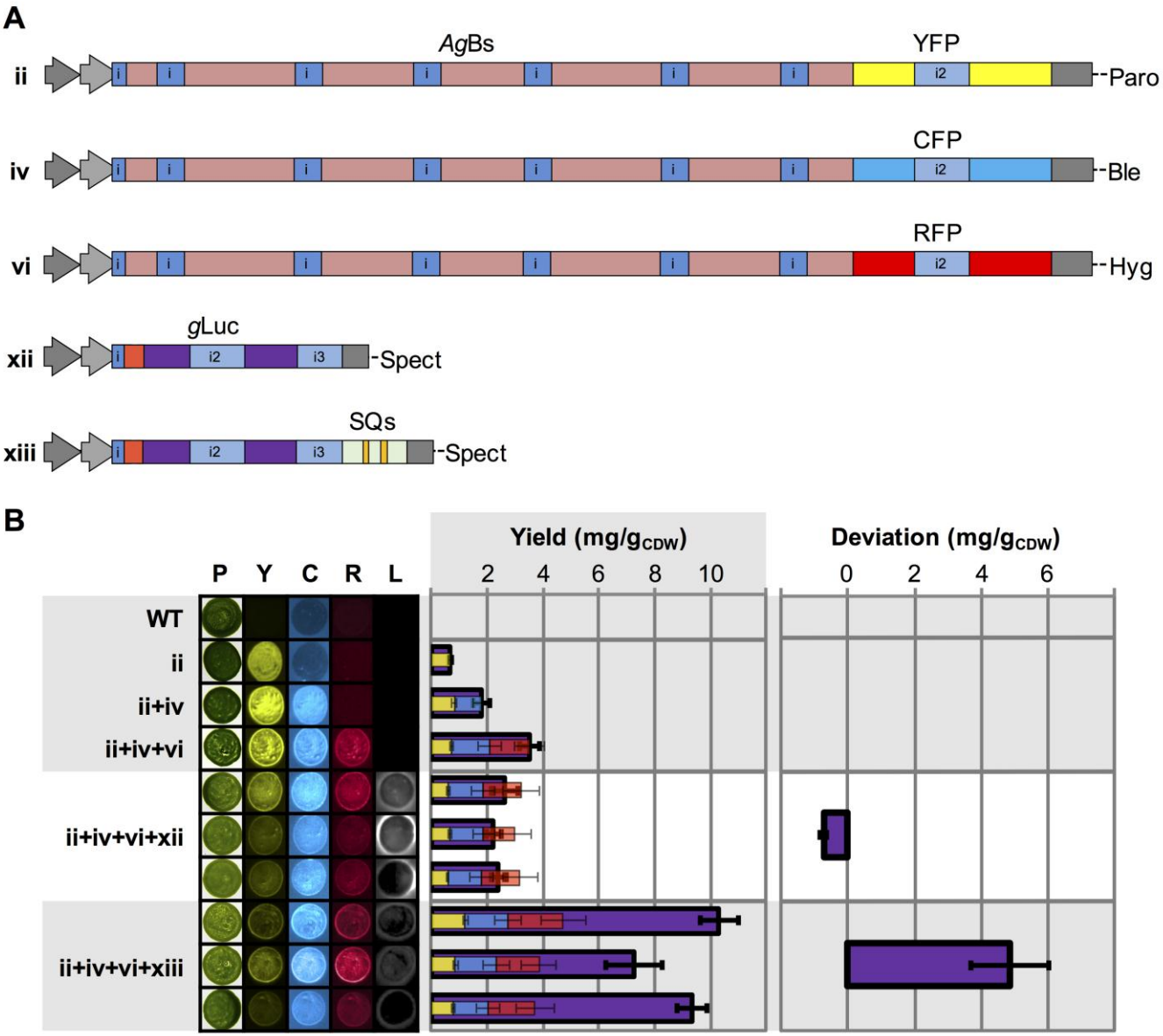

Fig. 6

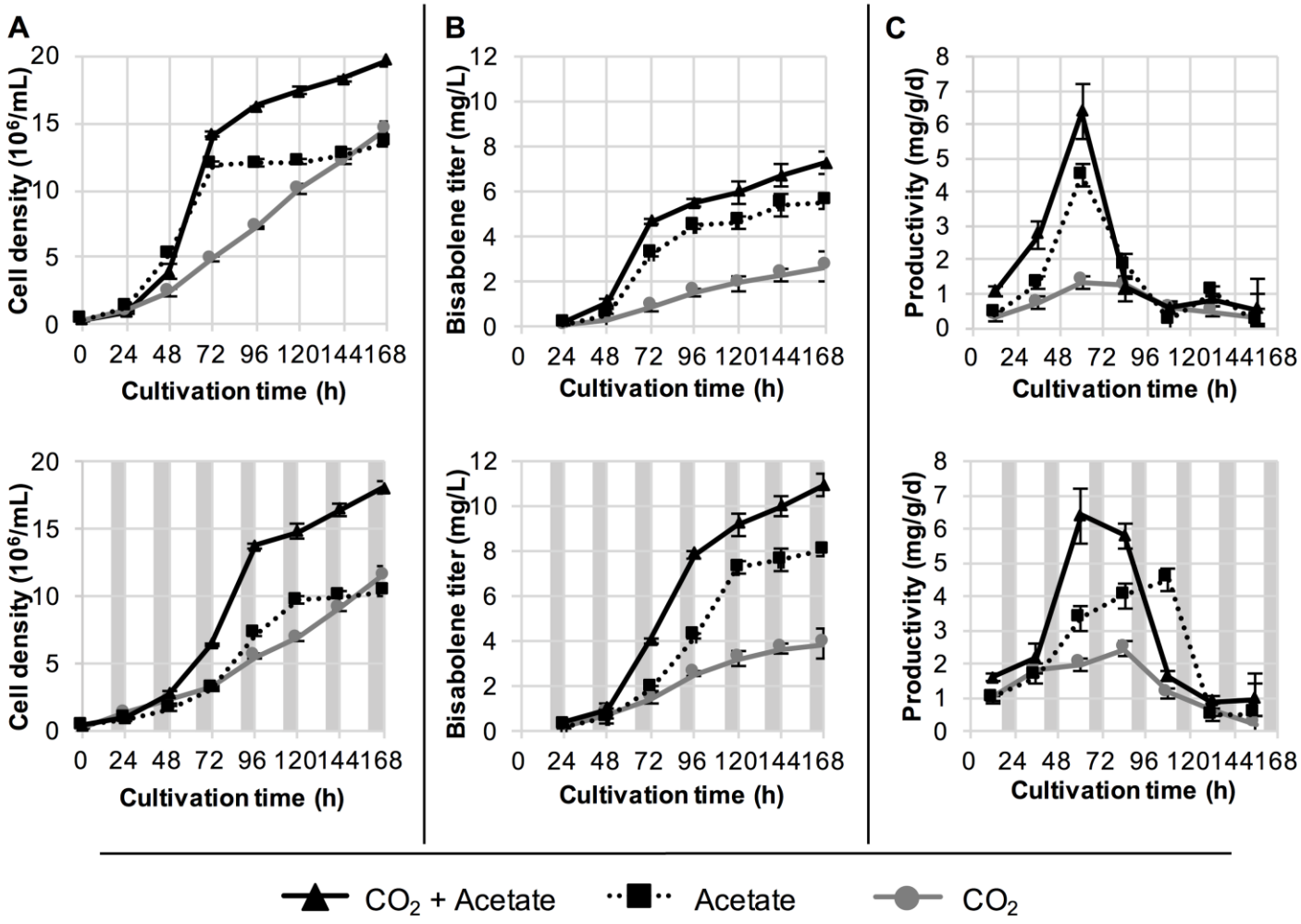

Fig. 7

Highlights

- Phototrophic production of heterologous bisabolene from *Chlamydomonas reinhardtii*
- Enhanced *Abies grandis* bisabolene synthase accumulation increases product yield.
- Identification of two gatekeeping enzymes for sesquiterpenoid metabolism
- 15-fold improved product yields by concerted metabolic engineering
- 11 mg L^{-1} bisabolene production from microalgal host